JCTC Journal of Chemical Theory and Computation

Article

pubs.acs.org/JCTC

Ions and RNAs: Free Energies of Counterion-Mediated RNA Fold Stabilities

C. H. Mak* and Paul S. Henke

Department of Chemistry, University of Southern California, Los Angeles, California 90089-0482, United States

ABSTRACT: We present an implicit ion model fo the calculation of the electrostatic free energies of RNA conformations in the presence of divalent counterions such as Mg^{2+}. The model was applied to the native and several non-native structures of the hammerhead ribozyme and the group I intron in *Tetrahymena* to study the stability of candidate unfolding intermediates. Based on a rigorous statistical mechanical treatment of the counterions that are closely associated with the RNA while handling the rest of the ions in the solution via a mean field theory in the Grand Canonical ensemble, the implicit ion model accurately reproduces the ordering of their free energies, correctly identifying the native fold as the most stable structure out of the other alternatives. For RNA concentrations in the range below 0.1 μM, divalent concentrations of ~0.5 mM or above, and over a wide range of solvent dielectric constants, the equilibrium number of divalent ions associated with the RNA remains close to what is needed to exactly neutralize the phosphate negative charges, but the stability of compact RNA folds can be reversed when the divalent ion concentration is lower than ~0.1 mM, causing the number of associated ions to underneutralize the RNA. In addition to calculating counterion-mediated free energies, the model is also able to identify potential high-affinity electronegative ion binding pockets on the RNA. The model can be easily integrated into an all-atom Monte Carlo RNA simulation as an implicit counterion model.

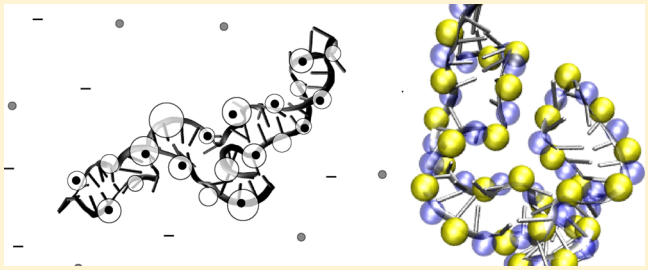

1. INTRODUCTION

Experimentally, it is well-established that the stability of RNA folds is strongly influenced by the concentration of divalent ions such as Mg^{2+}.[1−3] Theoretically, the understanding of how counterions mediate the effective attractive interactions that are needed to stabilize the structure of a RNA is incomplete. Although there are unique cases where the binding of divalent ions such as Mg^{2+} to specific sites on an RNA is important for establishing key tertiary interaction(s),[4−6] the divalent ion−RNA association seems to be nonspecific[7−9] for many others. From a practical point of view, the lack of a reliable theoretical model for RNA−ion interactions has hampered the computational studies of RNA folding/unfolding, because RNA fold stabilities are directed by the counterion-mediate electrostatic free energies. Because of the large Coulombic forces involved, RNA simulations including explicit divalent counterions are difficult to equilibrate. Consequently, there is a need for an implicit ion model, which is simple enough to be computed on the fly and yet realistic enough to reflect the stability of RNA folds accurately. This paper reports an effort along this direction.

There have been many theoretical attempts aimed at understanding the nature of the ion-mediated free energies experienced by nucleic acids in the presence of divalent counterions. Some of the earliest attempts were directed at explaining the stabilities of DNA bundles,[10−15] where the thermodynamic forces that mediate the effective attractions between rigid DNA molecules are thought to arise from correlated counterion fluctuations on different duplexes. There were also simulation evidence that flexible polyelectrolytes also show both interchain and intrachain attractions[16,17] in the presence of counterions. However, the existence and the precise nature of a possibly attractive effective intrachain interaction that could stabilize compact chain structures are still not completely clear.[18−20] However, it is increasingly clear that, for RNAs and multivalent counterions, the treatment of the electrostatic free energy by mean-field theories such as Poisson−Boltzmann is insufficient to correctly capture the counterion-induced effects.[3,9,21] Because of the strong electrostatic forces involved, the ions close to the RNA are often highly correlated, and a mean-field theory fails to describe the essential qualitative effects. This problem is exacerbated especially by higher-valency counterions.

In this paper, we develop a statistical mechanical model for RNA−ion interactions, using a consistent strategy to treat the strongly correlated counterions exactly, while employing a mean-field treatment for the ions in the diffuse charge cloud around the RNA. This allows us to both describe the equilibrium association of the counterions onto the RNA as well as compute the ion-mediated electrostatic free energy of any RNA conformation. A numerically feasible method has been devised to solve the statistical mechanics and calculate the free-energy difference between different RNA conformations so that the model may be integrated into an all-atom RNA simulation as an implicit ion model. In this paper, we have

Received: January 25, 2012
Published: October 16, 2012

   dx.doi.org/10.1021/ct300760y | *J. Chem. Theory Comput.* 2013, 9, 621−639

adopted a particularly simple model to describe the ion interaction sites on the RNA similar to what is often used in coarse-grained or tight-binding models for electrostatics,[22−24] but our model can easily be extended to include more atomic details on the RNA. Section 2 will describe our RNA−ion model, as well as the mean-field treatment of the unassociated ions and the Monte Carlo treatment of the associated counterions. Section 3 will discuss the equilibrium between associated and unassociated ions. Section 4 shows how the free-energy difference between two RNA conformations may be computed, and Section 5 applies the formulation to the native and non-native conformations of two example systems: the *Schistosoma* hammerhead ribozyme and the group I intron in *Tetrahymena*.

2. THE RNA-ION MODEL

At a sufficiently low RNA concentration, we consider placing one RNA molecule in a box of volume V to match its desired molarity. The rest of the box is filled with a solvent with a dielectric constant ε, and dispersed throughout it are the positive and negative ions. The box is coupled to a infinitely large ion reservoir with positive and negative ion concentrations c_+ and c_-, respectively.

The Hamiltonian of the system is

$$H = H_R + H_X + U_{RX} \tag{1}$$

where the Hamiltonian of the RNA is

$$H_R = \sum_\alpha \frac{|\mathbf{P}_\alpha|^2}{2M_\alpha} + U_R(\mathbf{r}_1, \mathbf{r}_2, \cdots) \tag{2}$$

where $\mathbf{P}_\alpha$ is the momentum of the αth RNA atom, M_α is its mass and the potential U_R is a function of the coordinates $\{\mathbf{r}_\alpha\}$, the Hamiltonian for the solution containing the position and negative ions is

$$H_X = \sum_j \frac{|\mathbf{p}_j|^2}{2m_j} + U_X(\mathbf{x}_1, \mathbf{x}_2, \cdots) \tag{3}$$

where $\mathbf{p}_j$ is the momentum of the jth ion in the solution, m_α is its mass, and the potential U_X is a function of the ion coordinates $\{\mathbf{x}_j\}$. U_{RX} is the potential between the RNA and the ions. Since we are interested in studying electrostatic effects involving the RNA and the ions, we will separate the potential of the RNA into an electrostatic part U_R^e and a nonelectrostatic part U_R^{ne}, such that $U_R = U_R^{ne} + U_R^e$.

It will be convenient to work in a mixed ensemble where the RNA is treated canonically with a fixed number of molecules (i.e., one) within the box while the solution is treated in a Grand Canonical ensemble with a fluctuating number of ions at fixed chemical potentials μ_+ and μ_-. The partition function of this mixed ensemble is defined as

$$\Xi = \mathrm{Tr}_R \mathrm{Tr}_X^* \exp[-\beta(H_R + H_X + U_{RX} - \mu_+ N_+ - \mu_- N_-)] \tag{4}$$

where Tr_R denotes a classical canonical trace over the RNA coordinates $\{\mathbf{r}_\alpha\}$, Tr_X^* is a Grand Canonical trace over the ion coordinates $\{\mathbf{x}_i\}$, as well as over all possible positive and negative ion numbers N_+ and N_-, $\beta = 1/k_B T$ and k_B is the Boltzmann constant. The integral over the momenta in Tr_R is separable from the configurational integral over positions, which can be written as

$$\Xi_c = \int \mathrm{d}^3 r_1\, \mathrm{d}^3 r_2 \cdots \exp\{-\beta[U_R^{ne} + F(\mathbf{r}_1, \mathbf{r}_2, \cdots)]\} \tag{5}$$

where the ion-mediated free energy F is given by

$$\beta F(r_1, r_2, \cdots) \equiv \beta U_R^e - \ln \mathrm{Tr}_X^* \exp[-\beta(H_X + U_{RX} - \mu_+ N_+ - \mu_- N_-)] \tag{6}$$

For every conformation of the RNA, $\{\mathbf{r}_\alpha\}$, our objective is to evaluate F arising from a Grand Canonical ensemble average over the ions.

To be able to account accurately for the ions that are strongly correlated with the RNA, we must treat them distinctly from those in the diffuse charge cloud around the molecule. We imagine that there are certain places on the RNA where which positive counterions would be preferably drawn. Figure 1 depicts these possible ion interaction sites on the RNA schematically by the large open circles superposed on an image of a RNA chain conformation. We will call the positions of these ion interaction sites $\{\mathbf{s}_i\}$. Clearly, the phosphate groups should have some of the strongest affinities for high-valency counterions, such as Mg^{2+}. Therefore, a minimal model should incorporate at least as many ion interaction sites as there are phosphate groups. Ions that are associated to these sites interact strongly with the RNA and also with each other, because they are all close to the RNA backbone, and the correlations among them must be treated accurately. We can accommodate any number of additional interaction sites as needed. In the extreme case, we can tile the space around the RNA completely with interaction sites, turning the entire system into a lattice model for the ions. However, this would hardly be beneficial or necessary, since only the ions that are most strongly correlated with the RNA need to be treated explicitly this way. In Figure 1, the positive ions are represented by small filled circles. Some of them are shown as being associated to the ion interaction sites on the RNA, while the rest are as in the solution. Negative ions, depicted by minus symbols in Figure 1, are also present in the solution. Since the

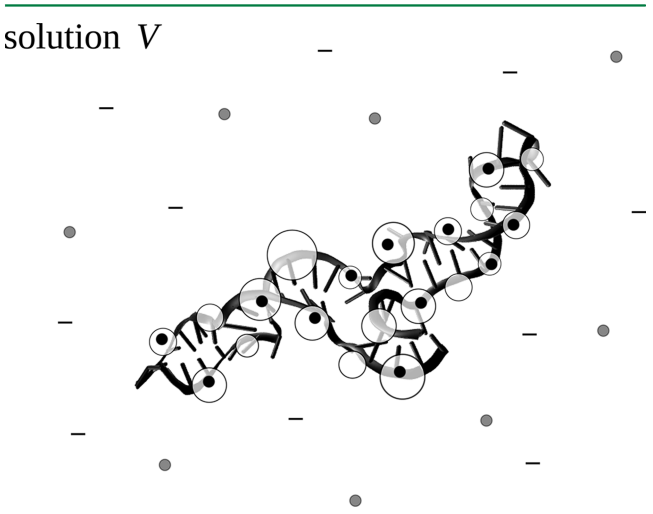

Figure 1. Schematic of the model. Cation interaction sites on the RNA are shown as open circles. The positive ions of charge z_+, shown as closed circles, are either associated with one of the interaction sites or in the diffuse charge close in the solution. Negative co-ions of charge z_- are indicated by minus symbols. The total RNA plus solution has a volume V. The system is coupled to an ion reservoir with positive and negative ion chemical potentials μ_+ and μ_-.

bare RNA is strongly negatively charged, we will consider only interaction sites for the positive ions on the RNA for simplicity, but the model can easily be extended to include interaction sites for negative ions also, if needed.

While this model is quite general, the focus of this paper is on non-site-specific ion−RNA interactions. In many RNAs, there are known specific ion interaction sites which are either important to the stability of the tertiary structures or to their chemistry. For example, in the hammerhead ribozyme, a magnesium binding site close to the catalytic core has been found to be important for its cleavage activity.[25−29] Similarly, in the P4−P6 domain of the *Tetrahymena* group I intron, the tertiary structure seems to nucleate around a Mg ion core aided by a tetraloop−receptor interaction.[30−35] In many of these cases, the key Mg ions involved are either chelated to specific atoms in the RNA or they are bound to specific sites on the RNA through hydration waters. While these site-specific ion−RNA interactions are critical for certain RNAs, there is another, more-generic class of ion−RNA interactions that do not appear to be site- or RNA-specific. The general observation that the structures of almost all RNAs can be stabilized by a divalent ion concentration in the millimolar range suggests that non-site-specific ion−RNA interactions is an important contributor to RNA fold stability, and these nonspecific interactions are believed to arise from correlated fluctuations in those counterions that are strongly associated with the RNA. In addition to these, the distributed counterion background in the solution can also interact with the RNA in the form of a diffuse charge cloud that is only loosely associated with the RNA. The formulation in this paper is aimed at modeling nonspecific ion−RNA interactions arising from both the correlated and diffuse counterions, but not the ones associated with specific sites, such as chelated ions, and those bound to the RNA through their solvation waters. However, we will also show in the examples below that certain gross features of site-specific ion−RNA interactions can be extracted from our calculations, even though the model is not specifically intended to address them. In our model, the ions in the diffuse charge cloud around the RNA will be handled effectively by a mean field approximation. This separation is justified when the number of ions associated to the interaction sites on the RNA is roughly sufficient to neutralize the negative charges on the phosphate backbone. In this case, the RNA plus its associated ions presents itself to the diffuse charge cloud as an overall approximately neutral object, and the resulting charge density fluctuations in the solution are expected to be weak. To segregate out these ions, we consider the dissociated ions in the solution as a separate subsystem from the associated ones. Notice that even though we have defined specific interaction sites on the RNA, our model does not necessitate any ion to actually be bound to the RNA. Since the two subsystems are both in equilibrium with the ion reservoir, the equilibrium number of associated ions will be controlled by the thermodynamic conditions as well as the system's physical parameters. Therefore, we can use our model to investigate shifts in the equilibrium distribution between the associated and unassociated ions as external conditions change.

Our model is aimed at understanding the electrostic free energy resulting from the association of divalent counterions to RNAs. Physiologically, the most relevant +2 ion is probably Mg^{2+}, while experimentally, ions such as Ca^{2+}, Sr^{2+}, Ba^{2+}, Mn^{2+}, and Cd^{2+} have shown nonuniversal effects. Our model is not sensitive to the chemical differences among these +2 ions, and it does not directly address specific ion-binding properties. Although parameters in the model, such as the size of the ion and its differential interaction strengths with different atomic sites on the RNA, can be calibrated to partially account for ion-specific binding effects, this will be left for future study. Since there is no explicit water in our model, it also will not address specific effects related to hydration, except through a dielectric continuum.

With the two ion subsystems defined, we can now divide $H_X + U_{RX}$ in eq 6 further. Based on the current RNA conformation $\{\mathbf{r}_\alpha\}$, we first define the positions of the ion interaction sites $\{\mathbf{s}_i\}$. To each possible ion interaction site i, we assign an occupation number:

$$\sigma_i = \begin{cases} 1 & \text{if ion interaction site at } \mathbf{s}_i \text{ is occupied by a } z_+ \text{ ion} \\ 0 & \text{otherwise} \end{cases} \tag{7}$$

When an unassociated ion leaves the solution and enters an ion interaction site, it is confined to a smaller free volume, compared to what is available to it in the solution. To properly account for this, we add a free-energy contribution each time an ion associates with the RNA of the form

$$\beta H_0 = \sum_i \beta\psi_i \sigma_i \tag{8}$$

where $\beta\psi_i = -\ln(\nu_i/\Lambda_+^3)$, ν_i is the effective free volume of ion interaction site i, $\Lambda_+ = h/(2\pi m_+ k_B T)^{1/2}$ is the thermal wavelength of a positive ion and m_+ is its mass. Furthermore, when a positive ion of charge z_+ is associated with interaction site i, it interacts with the partial charge q_α on each RNA atom α, as well as the associated ions on the other ion interaction sites. These interactions are given by

$$\beta H_1 = \frac{1}{2}\sum_{i\neq j}\sigma_i\sigma_j\frac{\lambda_B z_+^2}{|\mathbf{s}_i - \mathbf{s}_j|} + \sum_i \sigma_i \sum_\alpha \frac{\lambda_B z_+ q_\alpha}{|\mathbf{s}_i - \mathbf{r}_\alpha|} \tag{9}$$

where $\lambda_B = \beta e^2/4\pi\varepsilon_0\varepsilon$ is the Bjerrum length, e is the proton charge, ε_0 is the vacuum permittivity, and ε is the dielectric of the solvent. Because each RNA atom α has an impenetrable core, the unassociated ions cannot approach it closer than some critical distance b_α and the Hamiltonian must contain a hard-core interaction between every ion at position $\mathbf{x}_i$ and every RNA atom in the form

$$\beta H_2 = \sum_i \sum_\alpha \beta w_0 \theta(b_\alpha - |\mathbf{x}_i - \mathbf{r}_\alpha|) \tag{10}$$

where θ is the Heaviside function:

$$\theta(x) = \begin{cases} 0 & \text{if } x \le 0 \\ 1 & \text{if } x > 0 \end{cases} \tag{11}$$

and we let $w_0 \to \infty$. The charges on the RNA atoms and the associated ions around it present an electric potential to the unassociated ions (both positive and negative) in the solution in the form of

$$\beta V(\mathrm{x}) = \sum_\alpha \frac{\lambda_B q_\alpha}{|\mathbf{x} - \mathbf{r}_\alpha|}\theta(|\mathbf{x} - \mathbf{r}_\alpha| - b_\alpha) + \sum_i \frac{\lambda_B \sigma_i z_+}{|\mathbf{x} - \mathbf{s}_i|} \tag{12}$$

where the first term arises from the RNA atoms and the second term arises from the associated ions. In eq 12, we have included a step function that turns off the Coulombic interaction between a RNA atom and an unassociated ion when their distance is closer than the atom's hard core radius. (Because of

the presence of the hard-core interactions in H_2, this cutoff does not physically alter anything. However, in the mean field treatment of the unassociated ions below, the introduction of this cutoff will simplify the mathematics.) The interactions of the unassociated ions with themselves and with the RNA and its associated ions are included in the Hamiltonian:

$$\beta H_3 = \sum_j \frac{p_j^2}{2m_j} + \frac{1}{2}\sum_{i\neq j}\frac{\lambda_B z_i z_j}{|\mathbf{x}_i - \mathbf{x}_j|}, + \sum_i \beta V(\mathbf{x}_i) z_i \tag{13}$$

where $\mathbf{x}_i$ is the position of the ith unassociated ion and z_i is its charge (either z_+ for a positive ion or z_- for a negative one).

The ion-mediated RNA free energy in eq 6 can now be rewritten as

$$\beta F = \beta U_R^e - \ln \mathrm{Tr}_\sigma^* \exp[-\beta(H_0 + H_1 - \mu_+ N_\sigma) - \beta\Omega] \tag{14}$$

where Tr_σ^* denotes a trace over the occupation variables and $\{\sigma_i = 0,1\}$, $N_\sigma = \sum_i \sigma_i$ is the total number of associated (positive) ions. The effective free energy Ω for the occupation number configuration $\{\sigma_i\}$ induced by the unassociated ions is given by

$$\exp -\beta\Omega(\{\mathbf{r}_\alpha\}, \{\sigma_i\}) = \mathrm{Tr}_x^* \exp[-\beta(H_2 + H_3 - \mu_+ N_+ - \mu_- N_-)] \tag{15}$$

where Tr_x^* is a Grand Canonical trace over the unassociated ions, and N_+ and N_- are the number of unassociated positive and negative ions in the solution, respectively.

2.1. Mean Field Treatment of the Unassociated Ions. In this section, we will address the calculation of Ω. Using mean field theory, we will perform the trace over the unassociated ions, and at the end the mean field results, it will resemble a Poisson−Boltzmann theory or, when linearized, a Debye−Hückel treatment, of the unassociated ions. However, as pointed out by Zoetekouw and van Roij,[38,39] a consistent Grand Canonical treatment will also produce additional volume-dependent free-energy terms that are absent in the conventional canonical treatment. With very minor differences, our Grand Canonical mean field theory is similar to that given in their work.[38]

We want to compute the grand ensemble free energy Ω in eq 15 given a certain RNA conformation $\{\mathbf{r}_\alpha\}$ and associated ion configuration $\{\sigma_i\}$. To formulate a mean field theory for the unassociated ions in the grand ensemble, we start with the classical density functional theory expression for the free energy:[40]

$$\beta\Omega = \int \mathrm{d}^3x[z_+\rho_+(\mathbf{x}) + z_-\rho_-(\mathbf{x})]\beta V(\mathbf{x}) + \beta\mathcal{F}[\rho_+, \rho_-] \tag{16}$$

where $\rho_\pm$ are the positive and negative ion densities in the solution, $V(\mathbf{x})$ is the external potential and $\mathcal{F}$ is a functional of the ion densities not dependent on V. The "external" potential V, given by eq 12, is imposed on the unassociated ions by the RNA and its associated ions. According to density functional theory (DFT), the equilibrium densities $\rho_\pm$ are those that minimize the functional Ω:

$$0 = \frac{\delta\Omega}{\delta\rho_+(\mathbf{x})} = \frac{\delta\Omega}{\delta\rho_-(\mathbf{x})} \tag{17}$$

To proceed, we apply the standard mean field treatment[41] to derive an approximate expression for Ω:

$$\beta\Omega \approx \int_> \mathrm{d}^3x\rho(\mathbf{x})\beta V(\mathbf{x}) + \frac{\lambda_B}{2}\int_> \mathrm{d}^3x\mathrm{d}^3x'\frac{\rho(\mathbf{x})\rho(\mathbf{x})'}{|\mathbf{x}-\mathbf{x}'|} + \beta\mathcal{F}_{id}[\rho_+] + \beta\mathcal{F}_{id}[\rho_-] \tag{18}$$

where the charge density $\rho(\mathbf{x}) = z_+\rho_+(\mathbf{x}) + z_-\rho_-(\mathbf{x})$ and $\mathcal{F}_{id}$ is the free energy of an ideal solution of point ions,

$$\beta\mathcal{F}_{id}[\rho_\pm] = \int_> \mathrm{d}^3x\rho_\pm(\mathbf{x})\left(\ln\frac{\rho_\pm(\mathbf{x})}{c_\pm} - 1\right) \tag{19}$$

and $c_\pm$, the concentrations of the ions in the ion reservoir are related to their chemical potentials by $c_\pm = \Lambda_\pm^{-3}\exp(\beta\mu_\pm)$. In eqs 18 and 19, the greater than (">") signs on the integrals indicate that we have restricted the integrations to space *outside* the RNA atom cores. We can easily minimize eq 18, with respect to variations in $\rho_\pm$. If we define an effective potential ϕ as

$$\beta\phi(\mathbf{x}) = \lambda_B\int_> \mathrm{d}^3x'\frac{\rho(\mathbf{x}')}{|\mathbf{x}-\mathbf{x}'|} + \beta V(\mathbf{x}) \tag{20}$$

and the densities $\rho_\pm(\mathbf{x}) = c_\pm\exp[\mp\beta\phi(\mathbf{x})]$, minimizing $\beta\Omega$ will lead to a Poisson−Boltzmann equation for the charge density $\phi = z_+\rho_+ + z_-\rho_-$ outside the atom cores. The Poisson−Boltzmann equation can be solved numerically,[42−44] but since we need to solve it not only for every RNA conformation but also for every associated ion configuration $\{\sigma_i\}$, we will linearize the Poisson−Boltzmann equation to simplify it further. This leads to a Debye−Hückel theory for the unassociated ions, but as we have previously mentioned, other terms proportional to the volume, which are absent in the conventional Debye−Hückel theory, will also emerge in the Grand Canonical treatment below.

Expanding eq 19 to second order in $\rho_\pm$ gives

$$\beta\mathcal{F}_{id}[\rho_\pm] \approx V_f\overline{\rho}_\pm\left(\ln\frac{\overline{\rho}_\pm}{c_\pm} - 1\right) + \ln\frac{\overline{\rho}_\pm}{c_\pm}\int_> \mathrm{d}^3x\Delta\rho_\pm(\mathbf{x}) + \frac{1}{2\overline{\rho}_\pm}\int_> \mathrm{d}^3x[\Delta\rho_\pm(\mathbf{x})]^2 \tag{21}$$

where V_f is the free volume of the solution (the total volume minus the hard-core volumes of the RNA) and $\Delta\rho(\mathbf{x}) = \rho_\pm(\mathbf{x}) - \overline{\rho}_\pm$ is the deviation of the ion densities from their means defined by $V_f\overline{\rho}_\pm \equiv \int_> \mathrm{d}^3x\,\rho(\mathbf{x})$. Minimizing eq 18 with eq 21 yields two self-consistent equations:

$$0 = \ln\frac{\overline{\rho}_\pm}{c_\pm} + \ln\frac{\Delta\rho_\pm(\mathbf{x})}{\overline{\rho}_\pm} + z_\pm\beta\phi(\mathbf{x}) \tag{22}$$

In the above, the mean densities $\overline{\rho}_\pm$ inside the box are not necessarily equal to the limiting ion concentrations in the ion reservoir. The relationship between them is determined by integrating eq 22 over the entire box, giving

$$\overline{\rho}_\pm = c_\pm\exp(-z_\pm\beta\overline{\phi}) \tag{23}$$

and $\overline{\phi}$ is the integral of ϕ over the entire box. The parameter $\overline{\phi}$, in turn, is related to the physical parameters of the system via the neutrality of the system inside the box:

$$V_f[z_+c_+\exp(-z_+\overline{\phi}) + z_-c_-\exp(-z_-\overline{\phi})] = q_{RNA} + z_+\sum_i \sigma_i \tag{24}$$

where the right-hand side is the total charge of the RNA plus its associated ions, with q_{RNA} being the total charge of the RNA

dx.doi.org/10.1021/ct300760y | J. Chem. Theory Comput. 2013, 9, 621−639

($q_{RNA} = \sum_\alpha q_\alpha$). For every configuration of the associated ions, $\bar{\phi}$ can thus be determined before $\rho_\pm(\mathbf{x})$ is actually computed. However, before actually solving for $\rho_\pm$, eq 22 can also be substituted back into eq 21 to obtain a simpler expression for Ω. It is straightforward to show that

$$\beta\Omega = \frac{1}{2}\int_> d^3x \rho(\mathbf{x})\beta V(\mathbf{x}) - \left(\bar{\rho}_+ + \bar{\rho}_- + \frac{1}{2}\bar{\rho}\beta\bar{\phi}\right)V_f \tag{25}$$

where $\bar{\rho} = z_+\bar{\rho}_+ + z_-\bar{\rho}_-$ is the average of the total charge density. The second term gives rise to one of the free-energy contributions proportional to the volume.

To solve for $\rho_\pm$, we employ the two linear combinations: $\rho \equiv z_+\rho_+ + z_-\rho_-$ and $\zeta \equiv z_-\rho_+/\bar{\rho}_+ - z_+\rho_-/\bar{\rho}_-$, and use eq 23 to rewrite eq 22 as

$$\rho(\mathbf{x}) = \bar{\rho} - 2I\beta[\phi(\mathbf{x}) - \bar{\phi}] \quad \text{and} \quad \zeta(\mathbf{x}) = z_- - z_+ \tag{26}$$

which applies to the space outside the RNA atom cores and $I = {}^1/_2[z_+^2\bar{\rho}_+ + z_-^2\bar{\rho}_-]$ is the ionic strength of the solution. The second part of eq 26 is trivial, while the first part, being a linear integral equation in ρ, can be solved using Fourier transforms. However, since the integral for ϕ in eq 20 is restricted to space outside of the atom cores while the Fourier transform is performed over all space, we will add a core potential term in the form of $\int d^3x\rho(\mathbf{x}) \sum_\alpha \beta w_\alpha \theta(b_\alpha - |\mathbf{x} - \mathbf{r}_\alpha|)$ to eq 18 to expel the unassociated ion away from the RNA atom cores and extend the spatial integration to cover all space. Physically, adding this extra potential should not alter anything since there is already a hard wall potential in H_3 for all unassociated ions. Reminimizing Ω with this additional term leads to

$$\rho(\mathbf{x}) = \bar{\rho} - 2\beta I[\phi(\mathbf{x}) - \bar{\phi}] - \sum_\alpha \beta w_\alpha \theta(b_\alpha - |\mathbf{x} - \mathbf{r}_\alpha|) \tag{27}$$

which can now be solved by Fourier transform, yielding

$$\begin{aligned}\hat{\rho}(\mathbf{k}) = {} & \frac{2\pi(2I\beta\bar{\phi} + \bar{\rho})k^2}{k^2 + \kappa^2}\delta(\mathbf{k}) - \frac{4\pi}{k^2 + \kappa^2} \\ & \times \sum_i 2I\lambda_B(\sigma_i z_+)\exp(-i\mathbf{k}\cdot\mathbf{s}_i) \\ & - \frac{4\pi}{k^2 + \kappa^2}\sum_\alpha \exp(-i\mathbf{k}\cdot\mathbf{r}_\alpha)\left[\beta w_\alpha \frac{\sin(kb_\alpha)}{k}\right. \\ & \left. + (2I\lambda_B q_\alpha - \beta w_\alpha b_\alpha)\cos(kb_\alpha)\right]\end{aligned} \tag{28}$$

where $\hat{\rho}(\mathbf{k}) = \int d^3x \exp(-i\mathbf{k}\cdot\mathbf{x})$ and $\kappa = (8\pi I\lambda_B)^{1/2}$ is the reciprocal of the Debye screening length. While the first term in $\hat{\rho}$ does not contribute to $\rho(\mathbf{x})$, it will contribute to the free energy Ω and gives rise to one of the volume-dependent terms. The second term arises from the interactions of the charge density with the associated ions, and the third from interactions with the RNA atoms. Finally, setting each $\beta w_\alpha = 2I\lambda_B q_\alpha/(b_\alpha + \kappa^{-1})$ and inverse transforming $\hat{\rho}(\mathbf{k})$, we find that the charge density in the solution is a sum of one-particle densities, each one centered around a charge center, which is either a RNA atom having partial charge q_α and radius b_α or an associated ion with charge z_+ and radius 0:

$$\begin{aligned}\rho(\mathbf{x}) = {} & \sum_\alpha \rho^{(1)}(|\mathbf{x} - \mathbf{r}_\alpha|; q_\alpha, b_\alpha), \\ & + \sum_i \rho^{(1)}(|\mathbf{x} - \mathbf{s}_i|; \sigma_i z_+, 0)\end{aligned} \tag{29}$$

where

$$\rho^{(1)}(r; q, b) \equiv \begin{cases} 0 & \text{if } r < b \\ -\dfrac{q}{4\pi}\dfrac{\kappa^2\exp(\kappa b)}{1 + \kappa b}\dfrac{\exp(-\kappa r)}{r} & \text{otherwise} \end{cases} \tag{30}$$

Notice that, although the individual $\rho^{(1)}$ vanishes inside the RNA atom cores, their sum in eq 29 does leak into the cores. Substitution of eq 29 back into eq 25 and properly accounting for the $k = 0$ term in the $\hat{\rho}(\mathbf{k})$ yields the final expression for the free energy:

$$\begin{aligned}\beta\Omega = {} & \frac{1}{2}\sum_{\alpha\neq\gamma} q_\alpha q_\gamma\left[\beta u(|\mathbf{r}_\alpha - \mathbf{r}_\gamma|; b_\alpha, b_\gamma) - \frac{\lambda_B}{|\mathbf{r}_\alpha - \mathbf{r}_\gamma|}\right] \\ & + \frac{1}{2}\sum_{i\neq j}\sigma_i\sigma_j z_+^2\left[\beta u(|\mathbf{s}_i - \mathbf{s}_j|; 0, 0) - \frac{\lambda_B}{|\mathbf{s}_i - \mathbf{s}_j|}\right] \\ & + \sum_{i\alpha}\sigma_i z_+ q_\alpha\left[\beta u(|\mathbf{r}_\alpha - \mathbf{s}_i|; b_\alpha, 0) - \frac{\lambda_B}{|\mathbf{r}_\alpha - \mathbf{s}_i|}\right] \\ & + \frac{\lambda_B(2I\beta\bar{\phi} + \bar{\rho})}{2\kappa^2}(q_{RNA} + z_+\sum_i \sigma_i) \\ & - V_f\left(\bar{\rho}_+ + \bar{\rho}_+\frac{1}{2}\bar{\rho}\bar{\phi}\right)\end{aligned} \tag{31}$$

where the effective interaction u induced by the unassociated ions between two charge centers with hard-core radii b_1 and b_2 is

$$\beta u(r; b_1, b_2) = \begin{cases} 0 & \text{if } r < b_1 + b_2 \\ \dfrac{\exp[\kappa(b_1 - b_2)][1 + \exp(2\kappa b_2)]}{2(1 + \kappa b_1)} \times \dfrac{\lambda_B\exp(-\kappa r)}{r} & \text{otherwise} \end{cases} \tag{32}$$

Notice that u is asymmetric, with respect to b_1 and b_2, an artifact of the mean field approximation. Also, whenever $b_1, b_2 \ll \kappa^{-1}$, the screening length (eq 32) reverts to the standard Debye–Húckel result.[45] The first three terms in Ω correspond to the interactions of the RNA atoms with themselves, of the associated ions with themselves, and between the RNA atoms and the associated ions, respectively. The unscreened anti-Coulombic terms in Ω (i.e., those proportional to the reciprocal distances but with minus signs) will cancel the Coulombic interactions in the original RNA electrostatic potential U_R^e, as well as in the Hamiltonian H_1 and replace them with the screened interactions u given by eq 32.

2.2. Monte Carlo Treatment of the Associated Ions. While the calculation of Ω in eq 15 has been performed using a mean field approximation, the calculation of F in eq 14 will require an exact treatment because of the strong correlations involved. We will use a Monte Carlo simulation to explicitly carry out the ensemble average over $\{\sigma_i\}$. In this section, we will only address the calculation of Grand Canonical ensemble

dx.doi.org/10.1021/ct300760y | J. Chem. Theory Comput. 2013, 9, 621–639

averages, leaving the actual calculation of the free energy F to Section 4.

Using the expressions for H_0, H_1, and Ω above, the trace in eq 14 can be rewritten as

$$\exp(-\beta F) = \mathrm{Tr}_\sigma^* \exp[-\beta(H_\sigma - \mu_+ N_\sigma)] \tag{33}$$

where the effective Hamiltonian for the occupation numbers H_σ takes the general form

$$H_\sigma = \frac{1}{2}\sum_{i\neq j} \sigma\chi_{ij}\sigma_j + \sum_i \xi_i\sigma_i + h_\sigma \tag{34}$$

In eq 34, the two-body terms χ_{ij} come solely from the screened interactions in Ω of the associated ions with themselves

$$\chi_{ij} = z_+^2 u(|\mathbf{s}_i - \mathbf{s}_j|; 0, 0) \tag{35}$$

since the anti-Coulombic terms in Ω exactly cancel their Coulombic counterparts in H_1. The one-body terms ξ_i in eq 34 arise from the interactions of the associated ions with the RNA, after the anti-Coulombic terms in Ω cancel the Coulombic ones in H_1, together with the entropic factors in H_0, giving

$$\xi_i = z_+ q_\alpha u(|\mathbf{r}_\alpha - \mathbf{s}_i|; b_\alpha, 0) + \psi_i \tag{36}$$

Finally, h_σ results from the RNA−RNA interactions as well as the volume terms in Ω:

$$\beta h_\sigma = \frac{1}{2}\sum_{\alpha\neq\gamma} q_\alpha q_\gamma \beta u(|\mathbf{r}_\alpha - \mathbf{r}_\gamma|; b_\alpha, b_\gamma) + \frac{\lambda_B(2I\beta\bar{\phi} + \bar{\rho})}{2\kappa^2}(q_{RNA} + z_+ N_\sigma) - V_f\left(\bar{\rho}_+ + \bar{\rho}_+\frac{1}{2}\bar{\rho}\bar{\phi}\right) \tag{37}$$

where the first term represents the screened interactions among the RNA atoms left after the anti-Coulombic terms in Ω exactly cancel U_R^e. Notice that h_σ is not dependent on the individual occupation numbers but only on their total $N_\sigma = \sum_i \sigma_i$.

Equation 34 appears to have a Hamiltonian resembling a lattice-gas model. However, the parameters χ_{ij}, ξ_i, and h_σ are not constants. They all are dependent on the total number of associated ions (N_σ), which enters $\rho_\pm$, $\bar{\rho}$, and $\bar{\rho}$ in complicated ways. These, in turn, affect the magnitude of the screened Coulombic interactions u in eq 32. Therefore, when the number of associated ions N_σ changes in the simulation, all of the parameters χ_{ij}, ξ_i, and h_σ in H_σ will have to be re-evaluated. Even though it is somewhat cumbersome, this task is numerically quite manageable as long as the number of ion interaction sites on the RNA is not too large.

Any Grand Canonical ensemble average can now be calculated based on the trace in eq 34. For example, the ensemble average of the total occupation number is

$$\langle N_\alpha \rangle = \frac{\mathrm{Tr}_\sigma^* \exp[-\beta(H_\sigma - \mu_+ N_\sigma)N_\sigma]}{\mathrm{Tr}_\sigma^* \exp[-\beta(H_\sigma - \mu_+ N_\sigma)]} \tag{38}$$

The averaging of the type in eq 38 can be carried out using a standard Metropolis algorithm.[46] For the results presented in Section 3, a combination of two types of Monte Carlo (MC) moves were typically used. The first consisted of a single-site flip: If $\sigma_i = 1$, a new configuration where $\sigma_i = 0$ was considered, and vice versa. The second MC move consisted of a left or right cyclic permutation of a randomly selected block of sites. The first MC move alters the total number of associated ions N_σ, while the second conserves it. Starting with a random occupation number configuration, the system was first equilibrated, and statistics were then collected using several long MC simulations for each set of conditions.

3. ASSOCIATION EQUILIBRIUM OF COUNTERIONS TO THE RNA

In this section, we will discuss the results of Monte Carlo simulations using the RNA−ion model described in Section 2, with the hammerhead ribozyme as an example. In two previous studies,[36,37] we have investigated the possible conformational changes involved in the unfolding of the *Schistosoma* hammerhead ribozyme and have identified several characteristic gateway states between the native conformation and the unfolded three-way junction structure. We want to use the RNA−ion model here to evaluate the free-energy differences between these gateway states and the native structure to better understand their stabilities and what role the ions play in the folding sequence. In this section, we will first examine the equilibrium distribution of associated/unassociated ions for different RNA conformations under a variety of physical conditions. The actual calculation of their free energy differences will be addressed in Section 5.1.

The equilibrium partitioning of the counterions between their associated and unassociated states is key to the understanding of RNA fold stabilities. From the RNA−ion model above, we know that if there are no associated ions, the unfolded state of the RNA is highly favored. Even though the unassociated ions produce a screening of the electrostatic interactions of the RNA with itself, the overall effects of all the charges on the RNA still lead to a net repulsive self-interaction. While the Debye−Hückel screening reduces the strength of these interactions, it does not alter the overall sign of the electrostatic interactions, which remains predominantly repulsive. Therefore, fold stabilization within our model is impossible without associated ions. On the other hand, an overloading of associated counterions leads to the opposite result. If the total charge coming from the associated +2 ions is much larger than what is needed to neutralize the negative charge on the RNA, the overall net positive charge will give rise to a repulsion that again favors the unfolded structure. So if the ions are to be able to induce a net attractive self-interaction for the RNA, the number of associated ions must be somewhere between these two limits. But even that does not guarantee the existence of a net attractive self-interaction, the proof of which must come from a careful free-energy calculation, which we will present in Section 4. The remainder of this section will focus on the equilibrium partitioning of ions between their associated and unassociated states.

3.1. Placement of Ion Interaction Sites. Given each RNA conformation, we first need to decide where to locate the positive-ion interaction sites on the RNA. Since the negative partial charges are concentrated on the phosphate groups along the backbone, the simplest model is to assume that the strongest interaction sites for the positive ions are located near the phosphate groups. Since there is one phosphate per nucleotide, in a zero-order model, there should be as many ion interaction sites as the number of nucleotides in the RNA. For simplicity, we will assume that when a positive ion is associated with one of these sites, it is, on average, at a distance a from the P atom. Furthermore, we will assume that the negative charge of each phosphate group is concentrated on the P atom, giving each P atom a complete −1 charge. While this zero-order model seems rather crude, since we are focusing on nonspecific

dx.doi.org/10.1021/ct300760y | J. Chem. Theory Comput. 2013, 9, 621−639

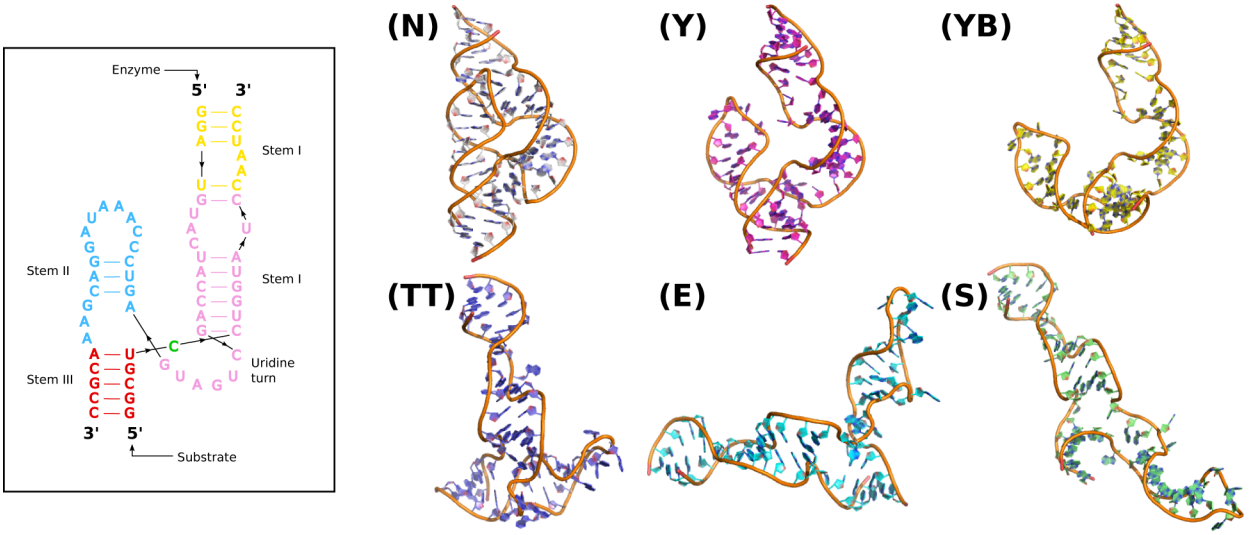

Figure 2. (Left) The two-dimensional (2D) structure of the *Schistosoma* hammerhead ribozyme.[36,37] (Right) Six structures of the hammerhead ribozyme considered in this paper. These structures were identified by a Monte Carlo simulation using large conformational moves as possible gateway structures to the unfolding of the hammerhead. (N) is the native tertiary structure. The other five have varying degrees of openness: (E) and (S) are the most extended, and (Y) and (YB) are the least open.

ion−RNA interactions, we do not expect the general nature of the RNA−ion interaction to be dependent very specifically on the atomistic details of the RNA structure, since the ability of multivalent ions to stabilize RNA folds seems to be quite generic.[2] Therefore, this zero-order model for the ion interaction sites on the RNA is a reasonable starting point. As we will see below, this simple model already captures many of the essential qualitative features of the RNA−ion interactions that are needed to properly discriminate the native fold from the unfolded conformations, and it also produces free energies that are quantitatively quite reasonable. If necessary, we can refine this zero-order model by introducing additional ion interactions sites, as well as accounting for the partial charges of the individual RNA atoms to try to produce better agreement with experiments or simulations.

For each Monte Carlo calculation, we consider a single conformation of the full-length *Schistosoma* hammerhead ribozyme[47] at a RNA concentration in the range of 10 nM to 10 μM. The counterions are +2 ions, and we assume the solution also contains added +2 ions (X^{2+}) and −1 ions (Y^{-}) with a XY_2 salt concentration ranging between 10 μM and 10 mM. The native conformation of the hammerhead, as well as five alternatives characteristic unfolded conformations that we have identified in previous large-scale Monte Carlo simulations,[36,37] are shown in Figure 2. In the full-length *Schistosoma* hammerhead, there are 61 phosphate groups. For each RNA conformation, we therefore position 61 ion interaction sites along the backbone, one at each P atom. As in the zero-order model, we place a full −1 charge on each P atom and assume that the average separation between it and a +2 ion associated with it is ∼3 Å, which is appropriate for a size similar to Mg^{2+}. For the calculation of the entropic factors ψ_i, we assume that each associated ion has a translational free volume corresponding to a 1-Å-thick spherical shell around each P atom. In the calculations, we have also examined the effect of the dielectric of the solvent by varying it between 1 and 80.

The two-dimensional (2D) structure of the hammerhead is shown on the left of Figure 2. The hammerhead is composed of two hybridized strands. Starting from the 5′ end, the longer strand is responsible for the enzymatic action of the molecule, while the substrate is the shorter strand with the scission site at C_{17} (colored green). The three-dimensional (3D) structures of some of the conformations we have studied by Monte Carlo are also shown in Figure 2. The native structure is labeled "N". The other five structures were identified by a Monte Carlo simulation using large conformational moves.[36,37] These five non-native structures are candidate intermediates along the different unfolding pathways, and they have various degree of openness, with "Y" being the most compact structure and "S" being the most extended. For each of them, we placed the ion interaction sites on the P atoms as described in Section 3.1 and performed a series of Monte Carlo studies according to the method delineated in Section 2.2 to calculate the equilibrium number of associated ions under a variety of different physical conditions. The results are presented in the next section.

3.2. Equilibrium Distribution between Associated and Dissociated Ions. For each of the six conformations in Figure 2, we have performed Monte Carlo simulations at different RNA and ions concentrations to study the equilibrium between associated and unassociated ions. All simulations were carried out for T = 298 K. Figure 3a shows results for the average number of associated ions, $\langle N_\sigma \rangle$, for a solution with a 0.1 μM RNA concentration in the native conformation (structure N in Figure 2) with various ion reservoir concentrations of the XY_2 salt, plotted as a function of the dielectric constant (ε) of the solvent. The four sets of data correspond to salt concentration ranging from 0.005 mM to 5 mM. In this and all other plots in this paper, the error bars are smaller than the size of the plotting symbols, unless otherwise indicated. The dashed line indicates the number of +2 ions that would exactly neutralize the RNA backbone, which is 30.5 in this case, since there are 61 phosphate groups on the hammerhead structure. As expected, when the +2 ion concentration c_+ in the reservoir is weak (c_+ < 0.05 mM), the equilibrium favors the unassociated ions. In contrast to this, higher +2 ion concentrations (c_+ < 0.05 mM) produce the opposite result, favoring associated ions instead. However, it is also clear that the equilibrium position is sensitive to ε. Especially for weak +2 ion concentrations,

dx.doi.org/10.1021/ct300760y | J. Chem. Theory Comput. 2013, 9, 621−639

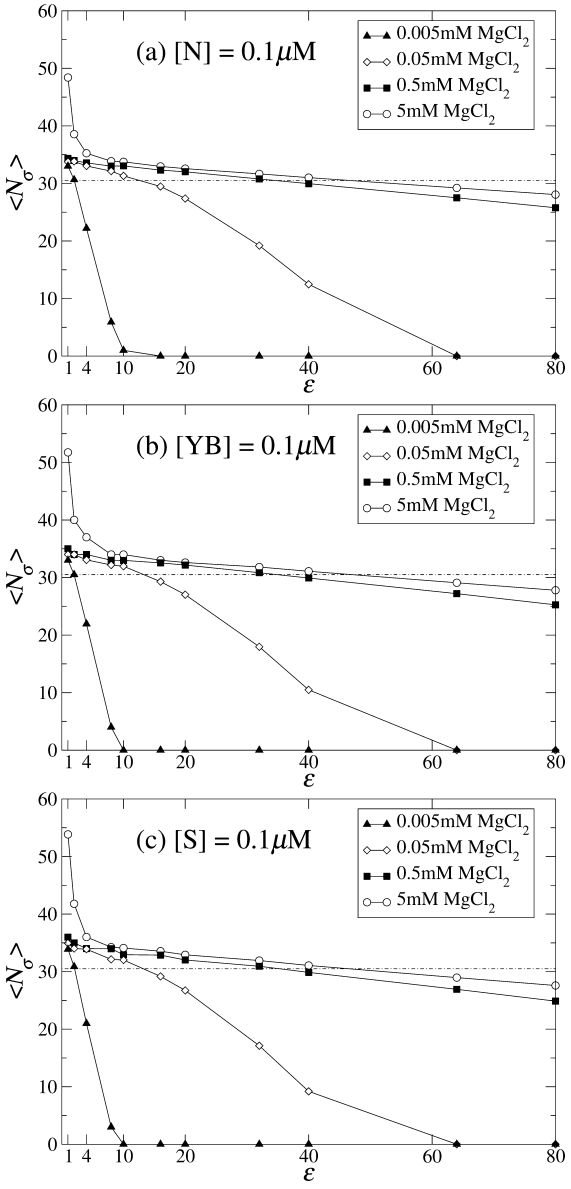

Figure 3. Monte Carlo results for the average number of associated ions $\langle N_\sigma \rangle$ for (a) the native structure N and two other conformations ((b) YB and (c) S). The concentration of the RNA in all three is 0.1 μM, while the $MgCl_2$ molarity ranges from 0.005 to 5 mM. The horizontal dotted line in each graph indicates the number of Mg^{2+} needed to exactly neutralize the RNA (30.5). $\langle N_\sigma \rangle$ is plotted as a function of the solvent dielectric constant (ε).

changing ε significantly shifts the distribution between associated and unassociated. On the other hand, when the +2 ion concentration is sufficiently high (c_+ = 0.5 mM and 5 mM in Figure 3a), the effect of changing ε is highly suppressed, except at extremely small ε values (less than ~4).

Comparing the results in Figure 3a for c_+ = 0.5 mM and 5 mM, it appears that when the concentration of +2 ions is in the range of 0.5 mM or above, the equilibrium distribution is firmly in favor of associated ions, to the extent that they approximately neutralize the RNA backbone charge, i.e. $\langle N_\sigma \rangle \approx 30.5$. Except for high +2 ion concentrations and very low dielectric solvents, $\langle N_\sigma \rangle$ remains very close to this value, indicating that the RNA and its associated ions form a roughly neutral entity for c_+ in the range of 0.5 mM or above. Since the physiological concentration of Mg_{2+} ions in the cell is estimated to be in the range of 0.1 to 1 mM[9] and this level of +2 ion concentration appears to be sufficient to stabilize most RNA tertiary structures, our Monte Carlo results seem to be quite reasonable. However, we should also mention that the physiological concentrations of different RNAs are not as well established; therefore, it is also important to examine how this associated/unassociated ion equilibrium is affected by the RNA concentration.

To address this question, we have performed additional Monte Carlo simulations at several different RNA concentrations. The results for two of them are shown in Figure 4. In

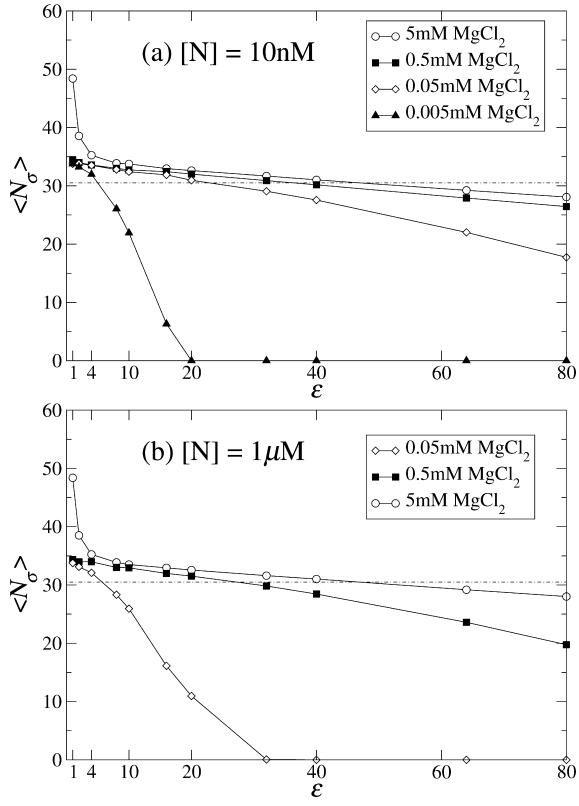

Figure 4. Plots showing the same Monte Carlo results as those observed in Figure 3 for two other RNA concentrations, 10 nM and 1 μM, for the native fold.

Figure 4a, $\langle N_\sigma \rangle$ is plotted against ε for the native conformation N at a concentration of 10 nM, which is 10 times smaller than that shown in Figure 3a. The two sets of results are qualitatively very similar, except the transition to the associated ionic state now occurs at lower concentrations of +2 ions. This is consistent with our expectation that a smaller RNA concentration should shift the equilibrium transition between associated and unassociated ions to lower ionic concentrations. But comparing the data for c_+ = 0.5 and 5 mM to those in Figure 3a, we see that the conclusion that we have reached above—that, at sufficiently high +2 ion concentrations, the ions are associated to the extent that they would roughly neutralize the RNA backbone—seems to hold true and remain unchanged for all lower RNA concentrations. Figure 4b shows the same results for a RNA concentration of 1 μM, which is 10 times larger than that in Figure 3a. In this case, the equilibrium position shifts in the opposite direction to higher ionic concentrations, which is consistent with expectations.

dx.doi.org/10.1021/ct300760y | J. Chem. Theory Comput. 2013, 9, 621−639

Returning to Figure 3, we examine the Monte Carlo results for other conformations. Two examples are shown in Figures 3b and 3c, at the same RNA concentration of 0.1 μM as observed in Figure 3a. Results in Figure 3b were obtained for the conformation labeled YB in Figure 2, whereas those in Figure 3c were for structure S. Compared to the native structure (N), which is the most compact, structure S is the most extended of the six conformations that we have studied and of all structures identified in the original conformational study of Mak et al.[36,37] Structure YB is a non-native structure between the two extremes.

As data in Figure 3 show, except for very minor differences, the equilibrium distribution of associated and unassociated ions are virtually indistinguishable among the three conformations, even though the compactness of their structures is vastly different. (The same conclusion could be reached for the other three conformations in Figure 2 and their Monte Carlo results will not be shown explicitly.) This suggests that upon the folding or unfolding of the RNA, the equilibrium number of ions associated to the RNA remains largely unchanged, as long as the concentration of the +2 ion is in the range of 0.1 mM or above.

3.3. Higher-Valency Counterions. In the literature, there is substantial agreement that the role that +1 counterions, such as Na^+ and K^+, play in stabilizing RNA folds is qualitatively different from that of +2 ions such as Mg^{2+}.[9] Although there are examples where Mg^{2+} can act as chelating ions on specific sites in certain RNAs,[6,30] the majority of folding studies on RNAs suggest that Mg^{2+} association is nonspecific, although the precise nature of how +2 ions stabilize RNA folds is still debated. The key difference between +1 and +2 counterions is their entropies. Because it takes half an many +2 ions to neutralize the same RNA, the association of +2 counterions causes less entropic penalty, and this leads to a qualitative difference between how +1 and +2 ions interact with the RNA.[11,14] A second factor is the size of the ion. Mg^{2+}, being a smaller ion than either Na^+ and K^+, is better able to hold onto its hydration waters stronger than Na^+ or K^+, even when associated with an RNA.[48] If this is true, aside from electrostatics, binding Mg^{2+} will be more favorable for the RNA than binding Na^+ or K^+, because the ion solvation shells will not have to be disturbed when Mg^{2+} binds. Notice that the model we have developed in this paper does not require a specific model for how the +2 ions bind. The only key assumption in our model is that the statistical mechanics of RNA−ion interactions is controlled by electrostatics but not by specific interactions. Even if Mg^{2+} binds as a hydrated ion, the primary interactions between the ions and the RNA remain electrostatic in nature, albeit possibly with a different dielectric constant. Our model can easily be extended to accommodate these necessary modifications. But even if the nonspecific association of Mg^{2+} to a RNA can be proven to be thermodynamically stable, binding itself does not necessarily imply that the ions are able to induce an effective interaction that could stabilize the tertiary structure of the RNA. This is why an accurate estimate of the free energies is crucial, and this will be addressed in Section 4.

If the association of +2 counterions to RNAs is nonspecific and they do give rise to stabilization of RNA folds, then one may speculate that the association of +3 of +4 ions would lead to even stronger stabilities.[9] Of the two key factors that influence association mentioned above, the entropic advantage of binding +3 ions versus +2 ions will be weaker than the difference between +1 ions and +2 ions, and the integrity of the hydration shell will be clearly dependent on the identity of the ion. To understand how changing to +3 counterions affect the statistical mechanics of the system, we have carried out Monte Carlo simulations using a fictitious ion X^{3+}, assuming that it has the same size and mass as Mg^{2+}. The results are shown in Figure 5 for a RNA molarity of 10 nM in the native

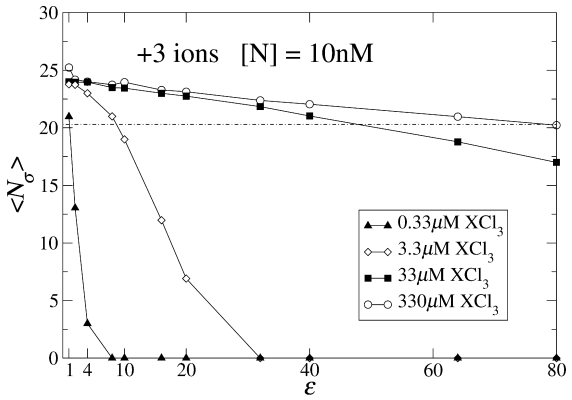

Figure 5. Plots showing the same Monte Carlo results as those observed in Figure 3 for the native fold with +3 counterions instead of +2. The number of ions needed to neutralize the RNA is 20.3, which is indicated by the dotted line.

conformation. Except for the fact that the number of +3 ions needed to neutralize the RNA backbone is reduced to ∼20 (indicated by the dashed line), these results are qualitatively very similar to those in Figure 4a with the same RNA concentration. Therefore, the nature of the effects behind the association of +3 counterions seems to be similar to that of the +2 ions. However, the ion reservoir concentrations used to obtained the data in Figure 5 are actually 10 times lower than those used in Figure 4a; therefore, as expected, the association of +3 ions is thermodynamically more stable than that of +2 ions.

4. FREE ENERGIES AND ION-MEDIATED RNA FOLD STABILITIES

While the Monte Carlo results in the last section can address the association of the ions to the RNA, the question of whether the associated ions are indeed able to produce the effective interactions required to stabilize the folded structure of an RNA can only be answered by calculating the difference in free energies between two RNA conformations. If this is indeed possible, we can integrate the simple model developed in this paper into a fully atomistic molecular dynamics or Monte Carlo simulation to calculate the counterion-mediated free energy without including explicit counterions or solvent molecules, giving the simulation an immense numerical and speed advantage. In our work, we are particularly interested in building this effective counterion model into our own Loops MC simulation program[37] to carry out large-scale RNA folding and unfolding simulations.

Before we go into the details of the free-energy calculations, we return to one of the key observations made in Section 3 from Figure 3. We noticed that the ion-association characteristics are very similar among all the different RNA conformations. While the Grand Canonical simulations in Section 3 enable us to study ion association, during the course of the folding or unfolding of an RNA, the number of

dx.doi.org/10.1021/ct300760y | J. Chem. Theory Comput. 2013, 9, 621−639

associated ions remains essentially close to neutralizing condition. Therefore, once we have determined $\langle N_\sigma \rangle$ using the Grand Canonical Monte Carlo simulation above for the desired RNA and ion concentrations, we can then switch to a canonical ensemble for the counterions using a fixed N_σ equal to $\langle N_\sigma \rangle$ to study the folding or the unfolding of the RNA. This is advantageous because, in the effective Hamiltonian described by eq 34 for the associated ions, the factors χ_{ij}, ξ_i, and h_σ are N_σ-dependent. In the Grand Canonical simulations, when the number of associated ions changes, all these factors must be recomputed. But if N_σ is constant during the folding or the unfolding of the RNA, then the parameters in eq 34 are fixed and the corresponding Monte Carlo simulation in the canonical ensemble would be computational much more efficiently. This is particularly important if this calculation is to be integrated into an atomistic RNA simulation as the solvent model, because the algorithm must be fast enough to be called every time step.

4.1. Monte Carlo Calculation of the Free Energy. In the canonical ensemble for the associated ions where N_σ is fixed, the parameters χ_{ij}, ξ_i, and h_σ in the effective Hamiltonian for the associated ions H_σ in eq 34 are constants for a given RNA conformation $\{\mathbf{r}_\alpha\}$. To emphasize this, we will write them as $\chi_{ij}(R)$, $\xi_i(R)$, and $h_\sigma(R)$, where R denotes a RNA conformation $\{\mathbf{r}_\alpha\}$, so that the effective Hamiltonian for the occupation numbers $\{\sigma_i\}$ is a function of R:

$$H_\sigma(\{\sigma_i\}; R) = \sum_{ij} \frac{1}{2}\chi_{ij}(R)\sigma_i\sigma_j + \sum_i \xi_i(R)\sigma_i + h_\sigma(R) \tag{39}$$

To compare the stabilities of two RNA folds R_a and R_b, we must compute the free-energy difference $\Delta F = F(R_b) - F(R_a)$ between the two conformations, with F being given by eq 33 and the Grand Canonical trace Tr_σ^* replaced by a canonical one at fixed N_σ.

To calculate ΔF, we employed the Bennett acceptance ratio (BAR) method.[49] For this, we ran two parallel simulations: one on $H_\sigma(R_a)$, to generate a Monte Carlo sampling of the occupation number configuration $\{\sigma_i\}_a$; and the other on $H_\sigma(R_b)$, generating a sampling of $\{\sigma_i\}_b$. Both simulations are determined at the same fixed N_σ. Periodically, we considered switching the instantaneous occupation number configuration $\{\sigma_i\}_a$ from one RNA conformation R_a to R_b with the Metropolis acceptance probability,[46]

$$P(a \to b) = \min(1, \exp[-\beta[H_\sigma(\{\sigma_i\}_a; R_b) - H_\sigma(\{\sigma_i\}_a; R_a)]]) \tag{40}$$

and vice versa. The free-energy difference is given in the BAR method by the ratio

$$\exp(-\beta[F(R_b) - F(R_a)]) = \frac{\langle P(a \to b)\rangle_a}{\langle P(b \to a)\rangle_b} \tag{41}$$

where $\langle A\rangle_y$ denotes an ensemble average of A along Monte Carlo trajectory $\{\sigma_i\}_y$.

For the results presented below, a combination of two types of Monte Carlo moves were typically used. The first consisted of exchanging the occupation numbers between two sites. The second Monte Carlo move consisted of a left or right cyclic permutation of a randomly selected block of sites. Both MC moves conserve N_σ. Starting with a random occupation number configuration, the system was first equilibrated, and statistics were then collected using several long MC simulations for each pair of RNA conformations. In the following, we will demonstrate this using three specific examples.

5. ION-MEDIATED FREE ENERGIES AND RNA FOLD STABILITIES

5.1. The Hammerhead Ribozyme. Using the BAR method described above, we have computed the free-energy difference between every pair of the hammerhead conformations shown in Figure 2 with different number of associated +2 ions and at varying dielectric constants. For all of these calculations, the RNA concentration was 10 nM and the salt concentration was 0.5 mM. The results are summarized in Figure 6, where the free energy of each conformation, relative to the native fold (N), is plotted as a function of the dielectric constant ε. With 61 phosphate groups on the hammerhead and $z_+ = +2$, $N_\sigma = 30$ and 31 are the two associated ion numbers closest to neutralizing the RNA. For every RNA conformation, the ΔF shown in Figures 6a and 6b for $N_\sigma = 30$ and 31 are almost quantitatively identical. Moreover, Figure 6 reveals that the free energy for every non-native conformation is higher than the native structure, providing clear evidence that the model we have formulated is able to correctly identify the native structure as the lowest free-energy fold out of many vastly diverse alternative conformations, as long as the number of associated ions is close to neutralizing the RNA.

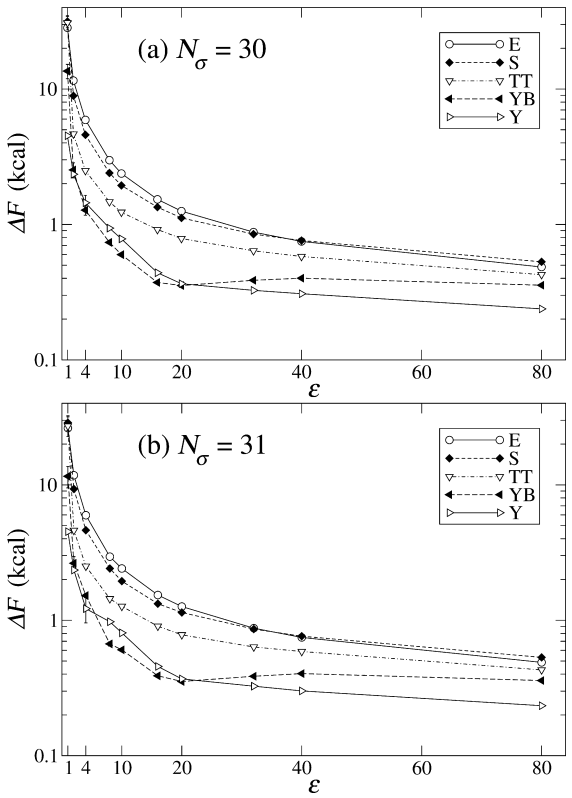

Figure 6. Monte Carlo results from canonical ensemble simulations using the BAR method to calculate the free-energy difference ΔF between each of the five non-native conformations in Figure 6 (E, S, TT, YB, and Y) and the native state. The data in panels (a) and (b) are for the two N_σ values, 30 and 31, closest to the number of +2 ions required to exactly neutralize the RNA. ΔF for the five non-native conformations indicate that the native fold is most stable and the extended structures (E) and (S) are the least stable.

dx.doi.org/10.1021/ct300760y | J. Chem. Theory Comput. 2013, 9, 621−639

The data in Figure 6a for N_σ = 30 are replotted in Figure 7 for several values of ε, showing more clearly how the

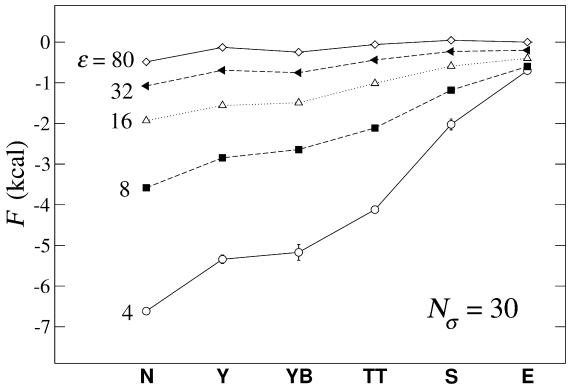

Figure 7. Free energies from Figure 6a replotted as a function of the six structures in Figure 2 for several values of the dielectric constant.

counterion-induced free energy F varies with structure. Of the six structures in Figure 2, the native conformation (N) is clearly the most compact, while E and S are the most extended. Other than these, conformation TT is more open than Y and YB. From Figures 6 and 7, the stability of each conformation is clearly seen to be correlated with the degree of openness of the structure. Structures E and S have the highest free energies, while structures YB and Y have free energies closest to that of the native state. Structure TT has intermediate free energy. This correlation between the stability of the fold to the compactness of its structure holds true over the entire range of the dielectric constant, from ε = 1 to ε = 80, although the relative stabilities of the structures can vary with ε (e.g., between Y and YB). Different measures of the compactness of these structures, including their radii of gyration and root-mean-square deviation (RMSD) from the native conformation, as well as the solvent-accessible surface areas (SASA), are given in Table 1. Since the free energy decreases when the structure becomes more compact, these results are consistent with the common view that the free-energy landscape can form a funnel to direct the folding of the RNA into its lowest free-energy native state.

Bulk measurements of the counterion-mediated free energy cannot be made for a specific conformation. This makes a direct comparison between the computed free energies and experiments difficult. Experimentally, the unfolding of a small RNA typically goes through a compact but disordered "intermediate state", which is often characterized by a collection of nonspecific structures; therefore, the experimental folding free energy does not necessarily correspond to the calculated free energy of any specific conformation. However, the folding free energy can provide an experimental validation for the order of magnitude of the calculated free energies. Draper et al. have analyzed experimental and theoretical free energy data for several small RNAs similar in size to the hammerhead.[6,54,55] For tRNA,[54] they attributed a free energy difference between the folded and the intermediate states of ~6 kcal/mol to the counterions, drawing evidence from previous experimental Mg^{2+} binding data from Romer and Hach.[56] For a 58-nucleotide fragment of rRNA,[6,55] they reported a somewhat larger ~10 kcal/mol free energy difference between the folded and the intermediate states coming from nonspecific Mg^{2+} association with the RNA. The magnitudes of these estimates are in very good agreement with our calculated free energies at low dielectric. Computing reliable ion-mediated electrostatic free energies for RNA folds can be a numerically demanding task. We have seen that, depending on ε, the free energies of the non-native structures are on the order of <1 kcal to ~10 kcal at room temperature. Given that the individual electrostatic interactions between charges can be 2 or 3 orders of magnitude stronger, these relatively minute free-energy differences must be the results of the cancellations of many large and counterbalancing terms, and computing them requires a high degree of computational effort, as well as numerical precision.

5.1.1. Ion–Ion Correlation and Other Ion Effects. Figure 8 shows typical occupancies of the ion interactions sites observed

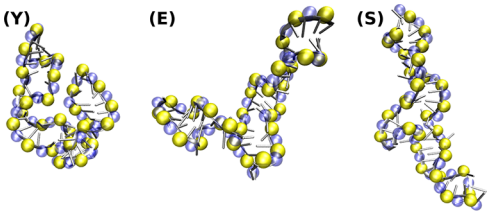

Figure 8. Snapshots showing representative configurations of the occupation of the ion interactions sites for three RNA conformations Y, E, and S by Mg^{2+} at ε = 10 and N_σ = 30. Occupied ion interaction sites are shown in yellow and unoccupied sites are shown in blue.

in the Monte Carlo simulations for three conformations (Y), (E), and (S) at a solvent dielectric ε = 10. Notice that the occupied (yellow) and unoccupied (blue) Mg^{2+} interaction sites tend to alternate along the backbone of the RNA, indicating that the ions when associating with the RNA attempt to organize themselves in such a way to try to minimize the repulsive Coulombic energy between closest neighbors. However, this alternating pattern does become less pronounced when ε is increased.

In Figure 9, we examine the effect of moving the associated ion number N_σ farther away from exactly neutralizing the RNA (30.5 in this case). Instead of a logarithmic scale, as observed in Figure 6, ΔF is plotted on a linear scale in Figure 9. The results for N_σ = 29 in Figure 9a shows a similar correlation between the stability of the fold with the compactness of its structure. The ordering of the stabilities of the five non-native structures

Table 1. Several Measures of Compactness of the Various Conformations of the Hammerhead Ribozyme: Radius of Gyration, Root-Mean-Square Deviation from the Native Structure, and Solvent-Accessible Surface Area

	Conformation					
measure of compactness	N	Y	YB	TT	S	E
radius of gyration, R_g (Å)	19.396	21.718	23.213	23.522	25.976	29.178
root-mean-square deviation, RMSD (Å)	0.000	6.393	9.805	13.255	15.441	20.832
solvent-accessible surface area, SASA (Å^2)	10568	12653	12956	13159	13229	13372

dx.doi.org/10.1021/ct300760y | J. Chem. Theory Comput. 2013, 9, 621–639

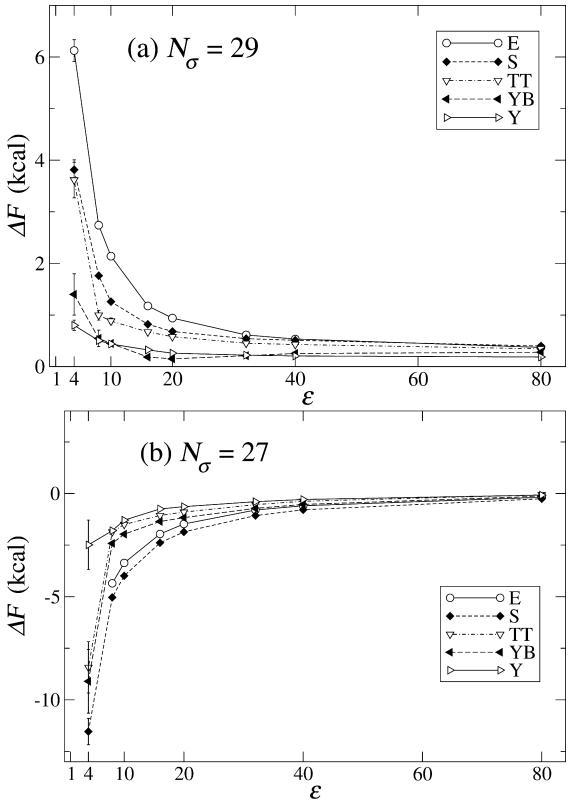

Figure 9. Monte Carlo results as in Figure 6 for ΔF of the five non-native structures at two values of N_σ farther away from what is needed to neutralize the RNA: (a) N_σ = 29, showing that the native state remains the most stable fold, and (b) N_σ = 27, where the native conformation has now become the least stable.

are similar to those in Figures 6a and 6b, but the overall magnitude of the free-energy differences appear to diminish when N_σ moves away from the number required to exactly neutralize the RNA. The results for N_σ = 32 are similar to those in Figure 9a and are not shown. In Figure 9b, we show results for N_σ = 27, which is farther away from the neutralizing condition. Now the free energies of all the non-native conformations become lower than the native structure, indicating that, far away from the neutralizing condition, the counterions actually destabilize the folded structure and the RNA will instead favor an open structure, unless it is counteracted by nonelectrostatic forces. This is consistent with experimental findings that, at low concentrations of +2 ions, RNAs are generally observed to unfold.[2] Therefore, the stability of the folded structure promoted by the counterions is favorable only when the number of associated +2 ions is close to neutralizing the RNA. However, as the results in Figure 3 show, there is a wide range of concentration conditions where $\langle N_\sigma \rangle$ meets this criterion; therefore, the stability of the folded structure seems to be fairly robust when the +2 ion molarity is near the physiological value of Mg^{2+} of ~0.5−1 mM.

We have also investigated the effects of using +3 counterions instead of +2 ions such as Mg^{2+}. The results are similar to the +2 ion data and therefore will not be displayed explicitly. For associated ion number N_σ = 20, which is close to neutralizing the RNA, and a XCl_3 concentration of 33 μM, the same trend similar to that observed for +2 ions in Figure 6 is seen, but the magnitude of the stabilization free energy for the native fold, relative to the open structures, is overall stronger for +3 ions.

5.1.2. Ion Titrations and Specific Ion Interaction Sites. Although the formulation of our model is intended to address nonspecific ion−RNA interactions, it is nonetheless interesting to determine whether information about specific ion binding sites on the RNA may be extracted from this simple model. This is important, because, in the full-length hammerhead ribozyme, a specific ion binding site near the catalytic core has been shown to be important to cleavage activity,[25,28,29] although its role in stabilizing the tertiary fold has not been firmly correlated with catalytic activities.[28] This putative ion-binding site is located within an electronegative recruiting pocket inside the folded structure.[29] Because our model captures the gross electrostatics of the system, we should also be able to identify any electronegative regions in the RNA that can serve as potential ion-binding sites. Demonstrating this ability provides further validation for the model.

Figure 10a shows the average occupancies, on an intensity scale, of the various ion interaction sites along the backbone of the hammerhead ribozyme in its native conformation, in a titration simulation where an increasing number of +2 ions (N_σ) are added to the system. A dielectric constant of ε = 10 was used, but similar results were observed for ε values between 4 and 20. We expect ion interaction sites in the neighborhood of the most electronegative region(s) in the RNA to be filled first, and as more +2 ions are titrated into the system, they should spread into other sites in the vicinity of these highly electronegative areas, and finally into the remaining available sites. Therefore, a careful ion titration simulation should be able to identify any potential ion recruiting pocket in the structure. As more +2 ions are titrated into the system, the ion−ion correlations (see Section 5.1.1) will eventually dominate the site occupancies, since like-charged divalent ions repel each other strongly. The results of the ion titration simulations in Figure 10a are thus consistent with these expectations.

According to the ion titration data in Figure 10a, with N_σ = 2 divalent ions, the first two ion interaction sites filled by them are sites 8 and 48. These two sites are shown in red in the native hammerhead structure on the right-hand side of Figure 10a. Site 48 is on residue C17 at the catalytic core of the hammerhead.[47] Previous ion occupancy studies[25,28,29] have shown that there is a specific ion binding pocket at the scission site between A9 and C17 of the hammerhead; therefore, the ion titration data are consistent with the identification of the region in the neighborhood of C17 as being the key ion recruiting pocket. The other high-occupancy ion interaction site with N_σ = 2 ions, site 8, is in the vicinity of the B4 cytosine near the interface between the stem I bulge/stem II loop interaction region. Tertiary interactions in this region are thought to be important for the stability of the tertiary fold of the full-length hammerhead structure.[47] While a specific ion-binding site has not been previously identified in this region, it is possible that the electrostatics in this region may facilitate a highly electronegative but nonspecific ion interaction pocket that helps to stabilize the tertiary structure.

In the second lane of Figure 10a, titrating N_σ = 5 +2 ions into the system leads to the filling of three other ion interaction sites: 20, 27, and 31. These are shown in orange in the native structure. Site 20 corresponds to the A9 residue at the catalytic core, which is in direct contact with C17. Therefore, the filling of site 20 following site 48 corroborates the suggestion that there is an electronegative binding pocket in the vicinity of the catalytic core. On the other hand, sites 31 and 27 correspond to the L5 uracil and the L1 cytosine, respectively, located near the

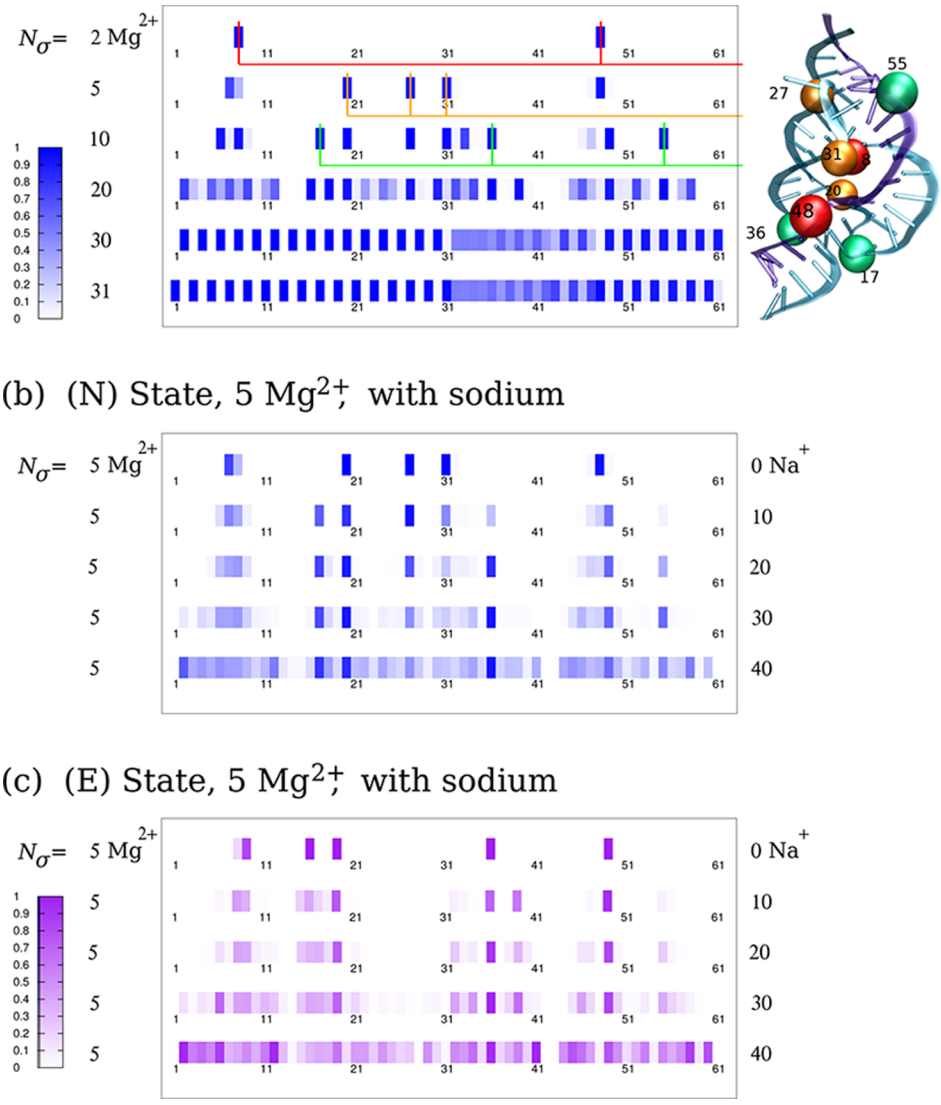

Figure 10. Mg^{2+} ion titration results for the hammerhead ribozyme at ε = 10: (a) native state (N) with increasing Mg^{2+} and no Na^+, revealing possible electronegative ion binding pockets as Mg^{2+} are titrated into the system; (b) native state (N) with 5 Mg^{2+} ions and different numbers of Na^+ ions (high-occupancy sites identified at low Mg^{2+} from panel (a) continue to be the most relevant when Na^+ is present); and (c) conformer E with 5 Mg^{2+} ions and different numbers of Na^+ ions.

stem I bulge/stem II loop interaction region. The occupation of these two sites following the filling of site 8 at the B4 cytosine on the stem I bulge again suggests that the stem I bulge/stem II loop interaction region is a second possible metal ion pocket on the hammerhead.

As more ions are added, the N_σ = 10 data reveal three more high occupancy sites: 17, 36, and 55. The locations of these are shown in green on the right-hand side of Figure 10a, and they are all in the neighborhood of the rest of the other high-occupancy sites. Therefore, the ion titration results suggest that there are two important electronegative regions on the hammerhead, which can potentially act as ion recruiting pockets. One is located at the catalytic core near residues A9 and C17. The other is in the stem I bulge/stem II loop region.

Experimentally, investigations of divalent ion binding are often carried out in high concentrations of monovalent ions such at Na^+ to ensure the stability of the tertiary structure of the RNA. When Na^+ are present, they may compete with Mg^{2+} ions for the electronegative binding pockets. Although the +2 charge of Mg^{2+} ions causes them to bind more favorably than Na^+, a sufficiently large Na^+ concentration can alter the chemical potential enough for the Na^+ to be able to outcompete the Mg^{2+} ions. Therefore, it is also important to study the robustness of the high-occupancy +2 ion sites that we have identified above when Na^+ ions are titrated into the system. Figure 10b shows the average ion interaction site occupancy for N_σ = 5 +2 ions in the presence of different numbers of Na^+ ions. The first lane in Figure 10b is identical to the second lane in Figure 10a with no Na^+ ions, while the remainder are titration results with increasing numbers of Na^+ ions. The high-occupancy sites identified using the data in Figure 10a, colored red, orange, and green, continue to be some of the most relevant, even in the presence of Na^+ ions. Among these, site 20, which corresponds to residue A9 at the catalytic core, is clearly the most robust. This is followed by site 48/49 at C17. On the other hand, the +2 ion occupancy at three other sites—8, 27, and 31 in the stem I bulge/stem II loop region—appear to become more diffuse as Na^+ ions are titrated in, but a significant density of +2 ions remains in their vicinity. This is consistent with the suggestion that we made previously, that

dx.doi.org/10.1021/ct300760y | J. Chem. Theory Comput. 2013, 9, 621−639

these sites may represent a more diffuse and nonspecific +2 ion binding pocket, whereas the ion recruiting pocket in the catalytic core is site-specific.

Finally, in Figure 10c, we show average +2 ion occupancies of the ion interaction sites for conformation E of the hammerhead (see Figure 2) in the presence of sodium. Comparing this to the data in Figure 10b for the N state, the +2 ion binding patterns of the two different conformations are clearly quite distinct, but, surprisingly, the ion interaction sites in the neighborhood of certain nucleotides also appear to have consistently high occupation in both conformations. These consensus high-occupancy regions are located at sites 19/20, which is near the A9 residue, at sites 48/49, which is near C17, and at site 36, which in near residue G12. In the native conformation, G12 is positioned directly against C17, and all three of these nucleotides are packed into the catalytic core in close proximity with each other. However, in conformation E, the catalytic core has been disassembled, and these three nucleotides are no longer near each other in 3D space. Interestingly, these nucleotides, which are directly involved in the catalytic activity of the hammerhead, receive intrinsically high +2 occupancy, even in the absence of an assembled catalytic core.

5.2. The Group I Intron in *Tetrahymena*. To demonstrate the robustness of our model we have also performed free-energy calculations on two larger systems: the *Tetrahymena* group I intron, as well as its standalone P4−P6 domain. The details of these calculations are similar to those for the hammerhead ribozyme described above.

5.2.1. P4−P6 Domain of the Group I Intron. The P4−P6 domain serves as an especially good target for this analysis. With 157 phosphate groups, it is roughly double the size of the hammerhead ribozyme. The full X-ray structure of the P4−P6 domain of the *Tetrahymena* group I intron is known (PDB ID: 1GID),[50] and this molecule has been studied extensively,[51,52] providing an opportunity to compare our results directly with experimental data.

The structure of the P4−P6 domain is composed of two helical stems connected by a hinge loop between the P5 and P5abc helices. Experiments have shown that the folding-unfolding process is dominated by the closing and opening of this hinge, while the major P4−P5−P6 and P5abc helices remain largely extended and undisturbed.[35] Therefore, the simplicity of this unfolding process suggests that intermediate structures are likely represented by conformations with varying degrees of hinge opening between the open and closed states. Using a Monte Carlo simulation that makes large conformational moves, we have identified several candidate conformations that are likely intermediates in the unfolding process. Some of these structures are shown in Figure 11, and they are labeled N for the native structure, and J, F, A, and O, from the most compact to the most open state. Measures of their compactness are given in Table 2.

Results of free energy calculations for N_σ = 78 and 79 are shown in Figure 12 for the P4−P6 domain. As with the hammerhead ribozyme, we once again find that the native state of the P4−P6 domain has the lowest free energy of all conformations and, thus, is the most stable, thermodynamically. Between ε = 4 and ε = 20, the most open state (O) is several kilocalories in free energy above the native state, and the magnitude of this value is consistent with previous estimates.[35]

While our model is not intended for studying specific ion binding sites, ion titration simulations can reveal where the electronegative pockets may be and help to identify potential

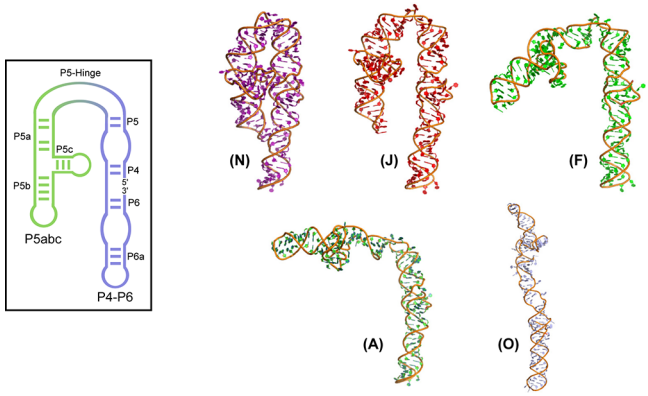

Figure 11. The six structures of the P4−P6 domain in the group I intron of *Tetrahymena* studied in this paper. The two-dimensional structure of the molecule is shown on the left. These six structures were found using large conformational Monte Carlo moves. The primary structural difference among these conformations is the variation of the P5-hinge angle. Conformations are realigned such that the P4 and P6 helix is oriented vertically, revealing the variation in their hinge angle.

Table 2. Various Measures of Compactness for the Different Conformations of the P4−P6 Domain

measure of compactness	Conformation				
	N	J	F	A	O
radius of gyration, R_g (Å)	29.990	33.257	38.641	48.010	57.041
root-mean-square deviation, RMSD (Å)	0.000	7.845	9.572	19.097	38.599
solvent-accessible surface area, SASA (Å^2)	24585	27239	27427	28933	28981

Mg^{2+} binding sites. This is particularly interesting for the P4−P6 domain since many experimental studies have focused on its folding due to the simplicity of its tertiary structure.[30,35] There are two essential tertiary interactions thought to be important in the native structure of the P4−P6 domain. The metal ion core on a bulge in the P5a region is believed to be able to bind multiple Mg^{2+} ions, causing an interaction with the metal core receptor on P4. There is also a GAAA tetraloop-receptor interaction between P5b and P6a[30] that appears to stabilize the fold.

Ion titration data shown in Figure 13a suggest that the two most electronegative ion association sites are located near residues 184 and 214. Site 184 is close to the metal ion core, while site 214, which is in close proximity to it, is on the other side on the P4−P6 helix situated near the ion core receptor. These two sites are colored red in the tertiary structure of the P4−P6 domain shown at the right-hand side of Figure 13a. These results provide strong evidence that the purported metal ion core is indeed one of the most electronegative ion recruiting pockets on the native conformation of this molecule.

Titrating more +2 ions into the system causes the additional ions to move into regions proximal to ion sites 141 and 164, shown in orange in Figure 13a. Sites 141 and 164 are both situated near the P5b/P5c junction, which apparently is the second-most electronegative region in the P4−P6 native structure, although no specific Mg^{2+} ion binding site has previously been reported here. As even more ions are titrated

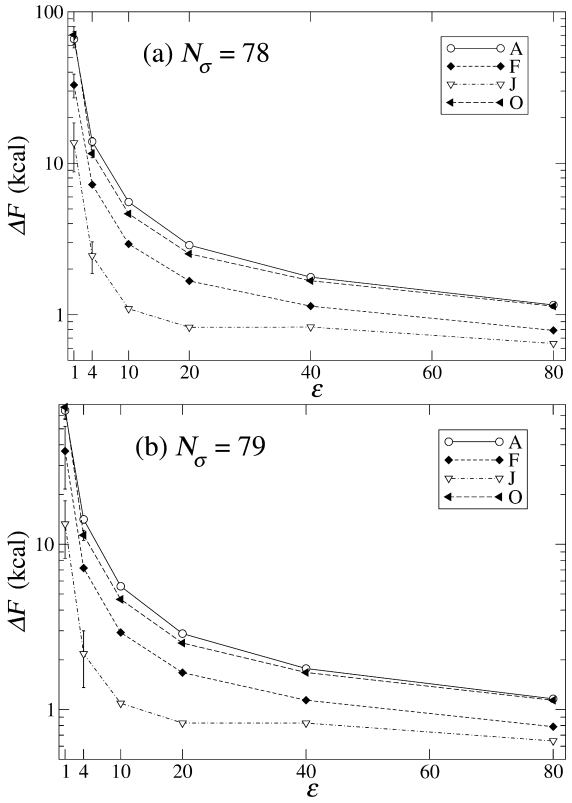

Figure 12. Monte Carlo results from canonical ensemble simulations using the BAR method to calculate the free-energy difference, ΔF, between each of the five non-native conformations in Figure 1 (J, F, A, O, and the native state (N)). The data in panels (a) and (b) are for N_σ = 78 and 79, respectively.

into the system, two effects are seen. First, more ions continue to enter the metal ion core-receptor region, in the surrounding of residues 183 to 188 and 212 to 214, as well as the P5b/P5c junction region around residues 141 and 164. But at the same time, a few other sites begin to be populated. They are colored green in Figure 13a. No specific ion-binding sites have previously been reported for these regions either, but they are located at seemingly critical positions in the tertiary structure of the P4−P6 domain to which ions associate and may be essential for the stability of the fold.

Experiments have also been performed aimed at ascertaining how many Mg^{2+} ions are acutally bound at the metal core. Some of these relied on determining the Hill coefficient,[34] which relates the folding free energy to the Mg ion concentration. These experiments are usually performed in a large background of Na^+ concentration to keep the folded structure intact. Titrating in Mg^{2+} ions then competes out Na^+ ions from the highest affinity binding sites and replace them with Mg^{2+}. Calculating the Hill coefficient by quantitatively simulating these experiments with mixed Na^+ and Mg^{2+} is not possible within our model for two simple reasons: (a) +1 counterions are expected to form a much more diffused ion cloud around the RNA, rather than being tightly associated like Mg^{2+}, and (b) in locating the Mg^{2+} ion association sites only near the phosphate P atoms, our model does not permit a precise determination of specific ion binding sites. However, as we have seen above for the hammerhead and from the +2 ion titration data for the P4−P6 domain, our model does capture the essential electrostatics properly and it can identify high +2 ion affinity regions on the RNA. It will therefore be interesting to try to estimate the average number of +2 ions bound in different regions on the RNA and to compare this against previous findings for the P4−P6 domain.

Simulations with five +2 ions and increasing numbers of Na^+ ions are shown in Figure 13b. The first lane, with no sodium, is identical to the second lane in Figure 13a. The rest show average ion associate site occupancies with increasing numbers

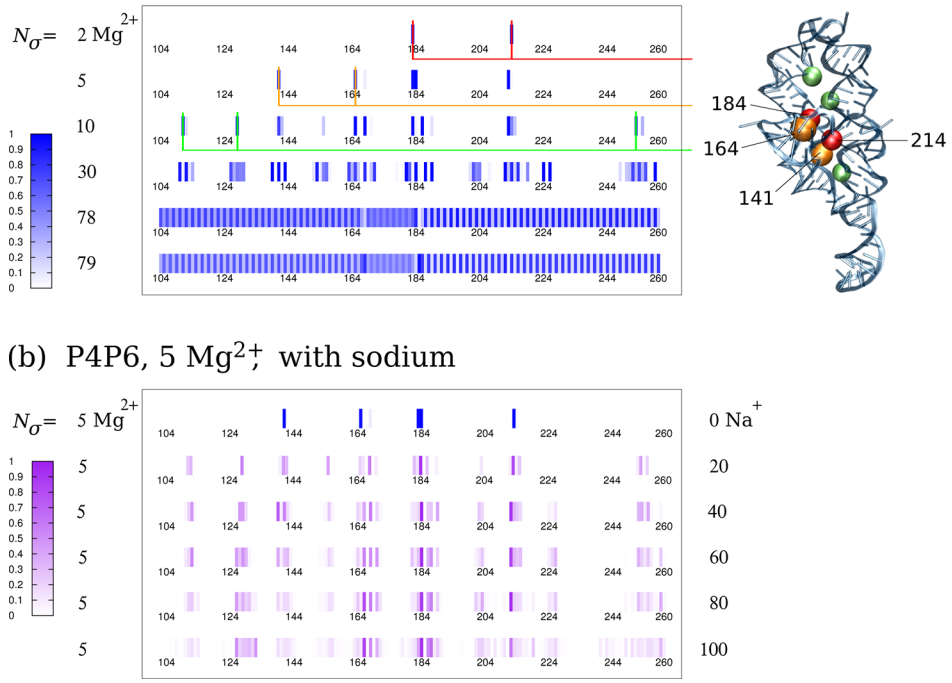

Figure 13. Mg^{2+} ion titration results for the P4−P6 domain of the *Tetrahymena* group I intron: (a) native state (N) with increasing numbers of Mg^{2+} ions and no Na^+ ions; and (b) native state (N) with 5 Mg^{2+} ions and different numbers of Na^+ ions.

dx.doi.org/10.1021/ct300760y | J. Chem. Theory Comput. 2013, 9, 621−639

Table 3. Average Mg^{2+} Occupancies within Different Neighborhoods in the Native (N) Conformation of the P4−P6 Domain with Five Mg^{2+} Ions from Simulated Ion Titration Experiments in Various Na^+ Backgrounds

	Number of Na^+ Ions							
neighborhoods in the (N) conformation	0	20	40	60	80	100	120	147
metal core/metal core receptor	2.95	2.03	1.77	1.76	1.74	1.74	1.45	1.40
P5b/P5c	2.01	1.62	1.54	1.30	1.30	1.15	0.92	0.82
tetralop/tetraloop receptor	0.00	0.50	0.69	0.80	0.79	0.88	1.12	1.28
P5 hinge	0.00	0.38	0.48	0.62	0.62	0.78	0.98	1.01

of Na^+ ions. The Na^+ ions compete with the +2 ion for these binding sites and, as the data show, they tend to smear out the +2 ion occupancies. This is expected because, when bound near a phosphate, a +1 ion renders that site neutral and reduces the electrostatics heterogeneity in its neighborhood. On the other hand, the +1 ion occupancies also fluctuate more than magnesium, because they are held less tightly. Figure 13b shows that the four electronegative regions identified in Figure 13a with five +2 ions but no Na^+ ions (first lane) continue to hold onto significant +2 ion populations when Na^+ ions are added, but additional +2 ion binding regions also open up when Na^+ ions are titrated into the system. In particular, the sites close to 124 are situated near the hinge opening on the J5/5a region, and they apparently receive a significant +2 ion population in the presence of Na^+ ions. Another cluster of +2 ion sites that develops with the addition of Na^+ are found near site 224 and between sites 244 and 260. These positions are near the tetraloop receptor on P6. Table 3 gives the average number of +2 ion within different regions of the native (N) conformation in the P4−P6 domain. Since our model is not designed to address specific ion binding, we have summed the ion occupancies on the sites within a small neighborhood of each region and displayed them as a function of increasing Na^+. For all cases, these four neighborhoods account for almost all five +2 ions in the system. While the metal core/metal core receptor region holds three +2 ions when no sodium is present, it seems to bind ∼1.75−2 +2 ions when Na^+ ions are present. On the other hand, while both the tetraloop/tetraloop receptor region and the P5 hinge region hold no +2 ions when sodium is absent, they seem to hold close to 0.8 +2 ions, each when Na^+ is present. The P5b/P5c junction also seems to take up close to one +2 ion with sodium. While no explicit estimate for the number of Mg^{2+} ions associated with other regions exist in the literature, there is evidence that the metal core/metal core receptor region holds anywhere from 2 to 4 Mg^{2+} ions[35] and the simulated ion titration data from our model are consistent with this observation.

Finally, to determine how the various potential ion binding pockets are taken over by Mg^{2+} ions under high Na^+ concentration, we show +2 ion titration data in Figure 14 for the P4−P6 domain in a background of Na^+ ions under almost-neutral conditions, such that the net charge in the system remains close to zero. Titrating in 1−5 +2 ions causes the various electronegative binding pockets to be filled differently. While the P5 hinge (orange) and the P5b/P5c (yellow) regions continue to gain +2 ion density, the occupancies at the metal core (red) and the tetraloop receptor (green) appear to saturate when the number of +2 reaches ∼5. Titrating in additional +2 ions does not substantially increase the ion occupancies at the metal core and the tetraloop receptor beyond 5. According to Table 3, the +2 ion occupancies at the metal core and the tetraloop receptor at saturation are ∼2 and ∼1, respectively.

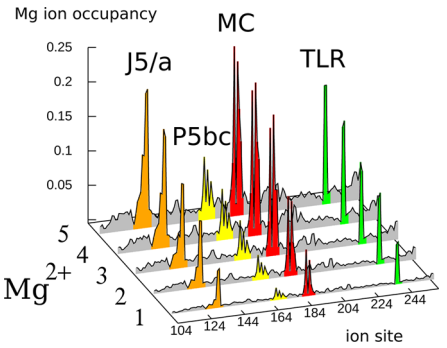

Figure 14. Ion titration results for the native conformer of the P4−P6 domain, with increasing number of Mg^{2+} ions and enough Na^+ ions to neutralize the RNA. Difference regions in the RNA are designated as follows: J5/a = P5 hinge, P5bc = P5b/P5c junction, MC = metal core, and TLR = tetraloop receptor. The Mg^{2+} ion occupancies at the P5 hinge and P5b/P5c regions appear to continue to rise as the number of Mg^{2+} ions increases, while the occupancies at the metal core and the tetraloop receptor regions seem to have reached saturation after ∼5 Mg^{2+} ions.

5.2.2. The Full Tetrahymena Group I Intron. As a final application of the effective counterion model and a complement to the study on the P4−P6 domain, we have also carried out calculations on the full *Tetrahymena* group I intron that has 246 residues. The full intron structure includes the P4−P6 domain previously discussed, as well as a P3−P9 domain, which is aligned perpendicularly in the native state. Again, several intermediate conformations were identified by large conformational Monte Carlo simulations, and their free energies were computed relative to the known native structure. These conformations are shown in Figure 15 and are labeled N, G, T, B, S, and O, in order from native to open.

Results of the free-energy calculations for N_σ = 121 and 123 are shown in Figure 16. (Table 4 shows the measure of compactness for different conformations of the group I intron.) Once again, the native state (N) proves to have the lowest calculated free energy. Although this molecule is nearly four times as large as the hammerhead, the complexity of the calculations is not much more demanding, compared to the hammerhead, and the effective counterion model that we have proposed can likely be applied to an RNA of even larger sizes without problem. Larger molecules do require more computational time, and we are exploring analytical methods to augment this effective counterion model in order to further improve its computational efficiency, so that it may be incorporated directly into all-atom folding/unfolding simulations of moderate-size RNAs.

5.3. Prospect for an Implicit Ion Model for All-Atom RNA Simulations. The question of whether the RNA−ion model introduced above can be incorporated into a full-scale RNA simulation as a viable implicit ion model will be

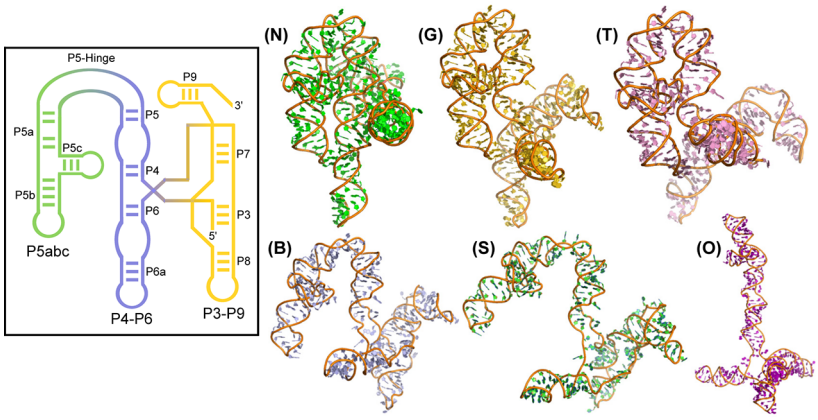

Figure 15. The six structures of the *Tetrahymena* group I intron. The 2-D structure is shown on the left-hand side. The full intron contains the P4−P6 domain previously analyzed, as well as several additional helices in the P3−P9 domain. The varying conformations being analyzed are shown on the right-hand side. These were found using large conformational Monte Carlo moves. For orientation, the P4, P5 helix remains vertical in each conformation shown. N denotes the native structure; G and T show twists in the P6 and P8 helices while the P5 helices remain static. B, S, and O retain those twists while the P5-hinge opens.

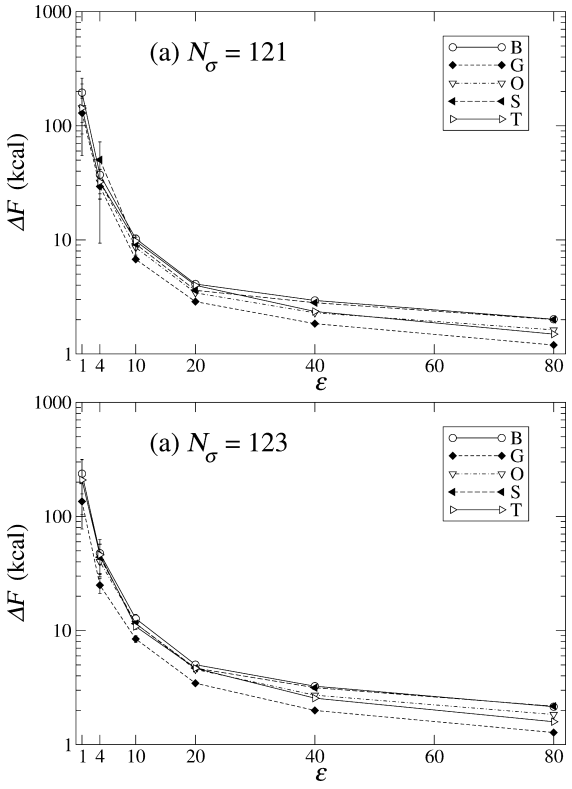

Figure 16. Monte Carlo results from canonical ensemble simulations using the BAR method to calculate the free-energy difference (ΔF) between each of the five non-native conformations in Figure 3 (B, G, O, S, T) and the native state (N). The data in panels (a) and (b) are for the two N_σ values (121 and 123). These data demonstrates that the native state is the most stable and also shows that this method remains effective, even with large molecules.

dependent on its accuracy and its speed. As Figure 6 shows, the free energies produced by the model follow what appears to be the correct order as a function of the compactness of the RNA structure, and it properly identifies the native fold as the most stable of all the alternatives. The magnitudes of the free-energy difference (ΔF) between each of the non-native folds and the native one are of the order of a few kcal/mol to <1 kcal/mol for ε = 4−80. In the model, a continuum dielectric constant has been assumed for the solvent and there is an ambiguity of what dielectric constant to use. One empirical approach to this question would be to try to either select the ε that best matches experimental thermodynamic measurements or the one that is best able to stabilize the native structure against all the other thermodynamic forces that favor the unfolded conformations (e.g., RNA conformational entropy). Another possible approach to this would be to refine the model to account for a possibly distance-dependent dielectric constant.[53] This work is currently underway.

Computational speed is another important consideration. The data in Figures 6 and, 9 were obtained using 1000 passes for equilibration and 10000 passes for the accumulation of the BAR free energy. To produce reliable ΔF with the BAR method for dielectric constants ε > 10, it is generally sufficient to use a few hundred passes for the accumulation, which on an AMD Phenom II X4 955 processor requires about 0.1 s of CPU time. We are currently investigating more efficiently alternative numerical algorithms to try to reduce this CPU requirement even further. For integration with molecular dynamics simulations, we also need to evaluate derivatives of the free energy. Since the BAR free energy is a noisy estimator, the computation of the derivatives of the free energy will require more numerical precision, and this is currently under study.

Table 4. Various Measures of Compactness for Different Conformations of the Group I Intron

measure of compactness	Conformation					
	N	G	T	B	S	O
radius of gyration, R_g (Å)	31.339	36.964	38.565	43.055	47.247	58.115
root-mean-square deviation, RMSD (Å)	0.000	11.401	17.574	24.176	29.080	51.847
solvent-accessible surface area, SASA (Å^2)	37959	42339	43689	47867	48418	45340

dx.doi.org/10.1021/ct300760y | J. Chem. Theory Comput. 2013, 9, 621−639

6. CONCLUSION

We have presented a statistical mechanical model to analyze the role of higher-valency counterions in their ability to help stabilize compact RNA folds. Using a combination of exact Monte Carlo calculations to handle the strongly correlated ions that are associated with the RNA and a mean-field treatment of the weakly correlated ones in the diffuse charge cloud around the RNA, we are able to accurately assess the equilibrium distribution between counterions that are closely associated with the RNA and the unassociated one. Under physiologically relevant RNA and +2 ion concentrations and a wide range of solvent dielectric, the number of +2 ions associated with the backbone of the RNA is close to the number needed to exactly neutralize the negative charges of phosphates on the RNA.

Using the model proposed, we have investigated the ion binding characteristics of partially or fully unfolded structures of the *Schistosoma* hammerhead ribozyme as well as the group I intron in *Tetrahymena*. It was found that the +2 ion association characteristics do not change appreciably when the hammerhead unfolds from the native state into the extended three-way junction structure. Similar conclusions were derived for +3 counterions.

More importantly, our RNA−ion model enables us to calculate the free-energy difference (ΔF) between any conformations due to the counterions and the co-ions. When coupled to an all-atom molecular dynamics or Monte Carlo simulation of the RNA, this will provide a simple but accurate implicit counterion model, allowing us to carry out RNAs simulations without having to explicitly simulate the ions. We used this method to evaluate the free-energy differences between partially or fully unfolded structures relative to the native fold, and found that every non-native structure has higher free energy, compared to the most compact native fold. Moreover, it appears that the more compact the fold, the lower its free energy. Therefore, the ion-mediated free energy seems to impart a directionality to the folding process, directing it to home into the native state. Our free energy calculations are based on the Bennett's acceptance ratio method, and it is sufficient fast to be able to be deployed in an all-atom RNA simulation. We are in the process of integrating this counterion model into our Loops MC simulation package.

In the future, there are two aspects of the model that we will particularly focus on improving. First, in the current formulation, we have assumed a uniform dielectric constant (ε) for the entire solvent. This ε value is used to describe both the ion−ion interactions as well as the interaction between the ion and the RNA. Since the bulk ε value is not reached unless there is a sufficient number of solvent molecules between the two interaction charges, assuming that the bulk dielectric constant ε applies to the interaction between the RNA and the counterion interaction sites on it could be problematic. Using a distance-dependent dielectric constant[53] would provide a more realistic alternative treatment.

Another possible improvement is to try to identify numerical techniques to accelerate the BAR calculation of the free energies. Currently, this requires a full Monte Carlo sampling on two RNA conformations in parallel. Even though this calculation is manageable for the hammerhead, which contains only 63 nucleotides, it will eventually become too expensive for larger RNAs. Therefore, a more-efficient numerical method for sampling the occupations of the ion interaction site must be sought in order for this method to be able to scale up to substantially larger systems.

AUTHOR INFORMATION

Corresponding Author

*E-mail: cmak@usc.edu.

Notes

The authors declare no competing financial interest.

ACKNOWLEDGMENTS

This material is based upon work supported by the National Science Foundation (NSF), under No. CHE-0713981.

REFERENCES

(1) Draper, D. E. A guide to ions and RNA structure. *RNA* **2004**, *10*, 335−343.
(2) Draper, D. E.; Grilley, D.; Soto, A. M. Ions and RNA folding. *Annu. Rev. Biopharm. Biomed.* **2005**, *34*, 221−243.
(3) Wong, G. C. L.; Pollack, L. Electrostatics of Strongly Charged Biological Polymers: Ion-Mediated Interactions and Self-Organization in Nucleic Acids and Proteins. *Annu. Rev. Phys. Chem.* **2010**, *61*, 171−189.
(4) Hanna, R.; Doudna, J. A. Metal ions in ribozyme folding and catalysis. *Curr. Opin. Chem. Biol.* **2000**, *4*, 166−170.
(5) Woodson, S. A. Metal ions and RNA folding: a highly charged topic with a dynamic future. *Curr. Opin. Chem. Biol.* **2005**, *9*, 104−109.
(6) Leipply, D.; Draper, D. E. Evidence for a thermodynamically distinct Mg^{2+} ion associated with formation of an RNA tertiary structure. *J. Am. Chem. Soc.* **2011**, *133*, 13397−13405.
(7) Heilman-Miller, S. L.; Thirumalai, D.; Woodson, S. A. Role of counterion condensation in folding of the *Tetrahymena* ribozyme. I. Equilibrium stabilization by cations. *J. Mol. Biol.* **2001**, *306*, 1157−1166.
(8) Koculi, E.; Hyeon, C.; Thirumalai, D.; Woodson, S. A. Charge density of divalent metal cations determines RNA stability. *J. Am. Chem. Soc.* **2007**, *129*, 2676−2682.
(9) Draper, D. E. RNA folding: Thermodynamic and molecular descriptions of the roles of ions. *Biophys. J.* **2008**, *95*, 5489−5495.
(10) Guldbrand, L.; Nilsson, L. G.; Nordenskiöld, L. A Monte Carlo simulation study of electrostatic forces between hexagonally packed DNA double helices. *J. Chem. Phys.* **1986**, *85*, 6686−6698.
(11) Ray, J.; Manning, G. S. An attractive force between 2 rodlike polyions mediated by the sharing of condensed counterions. *Langmuir* **1994**, *10*, 2450−2461.
(12) Lyubartsev, A. P.; Nordenskiold, L. Monte Carlo simulation study of DNA polyelectrolyte properties in the presence of multivalent polyamine ions. *J. Phys. Chem. B* **1997**, *101*, 4335−4342.
(13) Gronbech-Jensen, N.; Mashl, R.; Bruinsma, R.; Gelbart, W. Counterion-induced attraction between rigid polyelectrolytes. *Phys. Rev. Lett.* **1997**, *78*, 2477−2480.
(14) Ha, B. Y.; Liu, A. J. Counterion-mediated attraction between two like-charged rods. *Phys. Rev. Lett.* **1997**, *79*, 1289−1292.
(15) Diehl, A.; Carmona, H. A.; Levin, Y. Counterion correlations and attraction between like-charged macromolecules. *Phys. Rev. E.* **2001**, *64*, 011804.
(16) Stevens, M. J.; Kremer, K. The nature of flexible linear polyelectrolytes in salt free solution: A molecular dynamics study. *J. Chem. Phys.* **1995**, *103*, 1669−1690.
(17) Chu, J. C.; Mak, C. H. Inter- and intrachain attractions in solutions of flexible polyelectrolytes at nonzero concentration. *J. Chem. Phys.* **1999**, *110*, 2669−2679.
(18) Schiessel, H.; Pincus, P. Counterion-condensation-induced collapse of highly charged polyelectrolytes. *Macromolecules* **1998**, *31*, 7953−7959.
(19) Solis, F. J.; de la Cruz, M. O. Collapse of flexible polyelectrolytes in multivalent salt solutions. *J. Chem. Phys.* **2000**, *112*, 2030−2035.

(20) Lee, C.-L.; Muthukumar, M. Phase behavior of polyelectrolyte solutions with salt. *J. Chem. Phys.* **2009**, *130*, 024904.
(21) Chen, S.-J. RNA Folding: Conformational statistics, folding kinetics, and ion electrostatics. *Annu. Rev. Biophys.* **2008**, *37*, 197−214.
(22) Dryga, A.; Chakrabarty, S.; Vicatos, S.; Warshel, A. Coarse grained model for exploring voltage dependent ion channels. *Biochim. Biophys. Acta, Biomembr.* **2012**, *1818*, 303−317.
(23) Tan, Z.-J.; Chen, S.-J. Electrostatic correlations and fluctuations for ion binding to a finite length polyelectrolyte. *J. Chem. Phys.* **2005**, *122*, 044903.
(24) Tan, Z.-J.; Chen, S.-J. Ion-mediated nucleic acid helix−helix interactions. *Biophys. J.* **2006**, *91*, 518−536.
(25) Peracchi, A; Beigelman, L; Scott, E. C.; Uhlenbeck, O. C.; Herschlag, D. Involvement of a specific metal ion in the transition of the hammerhead ribozyme to its catalytic conformation. *J. Biol. Chem.* **1997**, *272*, 26822−26826.
(26) Kim, N; Murali, A; DeRose, V. J. Separate metal requirements for loop interactions and catalysis in the extended hammerhead ribozyme. *J. Am. Chem. Soc.* **2005**, *127*, 14134−14135.
(27) Vogt, M.; Lahiri, S.; Hoogstraten, C. G.; Britt, R. D.; DeRose, V. J. Coordination environment of a site-bound metal ion in the hammerhead ribozyme determined by ^{15}N and ^{2}H ESEEM spectroscopy. *J. Am. Chem. Soc.* **2006**, *128*, 16764−16770.
(28) Boots, J. L.; Canny, M. D.; Azimi, E.; Pardi, A. Metal ion specificities for folding and cleavage activity in the *Schistosoma* hammerhead ribozyme. *RNA* **2008**, *14*, 2212−2222.
(29) Lee, T.; Giambasu, G. M.; Sosa, C. P.; Martick, M.; Scott, W. G.; York, D. M. Threshold occupancy and specific cation binding modes in the hammerhead ribozyme active site are required for active conformation. *J. Mol. Biol.* **2009**, *388*, 195−206.
(30) Cate, J. H.; Hanna, R. L.; Doudna, J. A. A magnesium ion core at the heart of a ribozyme domain. *Nat. Struct. Biol.* **1997**, *4*, 553−558.
(31) Silverman, S. K.; Cech, T. R. Energetics and cooperativity of tertiary hydrogen bonds in RNA structure. *Biochemistry* **1999**, *38*, 8691−8702.
(32) Silverman, S. K.; Cech, T. R. An early transition state for folding of the P4−P6 RNA domain. *RNA* **2001**, *7*, 161−166.
(33) Takamoto, K.; Das, R.; He, Q.; Doniach, S.; Brenowitz, M.; Herschlag, D.; Chance, M. R. Principles of RNA compaction: Insights from the equilibrium folding pathway of the P4−P6 RNA domain in monovalent cations. *J. Mol. Biol.* **2004**, *343*, 1195−1206.
(34) Das, R.; Travers, K. J.; Bai, Y; Herschlag, D. Determining the Mg^{2+} stoichiometry for folding an RNA metal ion core. *J. Am. Chem. Soc.* **2005**, *127*, 8272−8273.
(35) Greenfeld, M.; Solomatin, S. V.; Herschlag, D. Removal of covalent heterogeneity reveals simple folding behavior for P4−P6 RNA. *J. Biol. Chem.* **2011**, *22*, 19872−19879.
(36) Mak, C. H.; Chung, W.-Y.; Markovskiy, N. D. RNA conformational sampling: II. Arbitrary length multinucleotide loop closure. *J. Chem. Theor. Comput.* **2011**, *7*, 1198−1207.
(37) Mak, C. H.; Loops, M. C. An all-atom Monte Carlo simulation program for RNAs based on inverse kinematic loop closure. *Mol. Simulat.* **2011**, *37*, 537−556.
(38) Zoetekouw, B.; van Roij, R. Volume terms for charged colloids: A grand-canonical treatment. *Phys. Rev. E* **2006**, *73*, 021403.
(39) Zoetekouw, B.; van Roij, R. Nonlinear screening and gas−liquid separation in suspensions of charged colloids. *Phys. Rev. Lett.* **2006**, *97*, 258302.
(40) Mermin, N. D. Thermal properties of inhomogeneous electron gas. *Phys. Rev.* **1965**, *137*, 1441−1443.
(41) Chaikin, P. M.; Lubensky, T. C. *Principles of Condensed Matter Physics*; Cambridge University Press: Cambridge, U.K., 2000; pp 204−208.
(42) Honig, B.; Nicholls, A. Classical electrostatics in biology and chemistry. *Science* **1995**, *268*, 1144−1149.
(43) Chin, K.; Sharp, K. A.; Honig, B.; Pyle, A. M. Calculating the electrostatic properties of RNA provides new insights into molecular interactions and function. *Nat. Struct. Biol.* **1999**, *6*, 1055−1061.
(44) Baker, N. A.; Sept, D.; Joseph, S.; Holst, M. J.; McCammon, J. A. Electrostatics of nanosystems: application to microtubules and the ribosome. *Proc. Natl. Acad. Sci. U. S. A.* **2001**, *98*, 10037−10041.
(45) Debye, P.; Huckel, E. The theory of electrolytes I. The lowering of the freezing point and related occurrences. *Phys. Z.* **1923**, *24*, 185−206.
(46) Metropolis, N.; Rosenbluth, A. W.; Rosenbluth, M. N.; Teller, A. H.; Teller, E. Equation of state calculations by fast computing machines. *J. Chem. Phys.* **1953**, *21*, 1087−1092.
(47) Martick, M.; Scott, W. G. Tertiary contacts distant from the active site prime A ribozyme fromor catalysis. *Cell* **2006**, *126*, 309−320.
(48) Ikeda, T.; Boero, M.; Terakura, K. Hydration properties of magnesium and calcium ions from constrained first principles molecular dynamics. *J. Chem. Phys.* **2007**, *127*, 074503.
(49) Bennett, C. H. Efficient estimation of free energy differences from Monte Carlo data. *J. Comput. Phys.* **1976**, *22*, 245−268.
(50) Cate, J. H.; Gooding, A. R.; Podell, E.; Zhou, K.; Golden, B. L.; Kundrot, C. E.; Cech, T. R.; Doudna, J. A. Crystal structure of a group I ribozyme domain: Principles of RNA packing. *Science* **1996**, *273*, 1678−1685.
(51) Murphy, F. L.; Cech, T. R. An independently folding domain of RNA tertiary structure within the *Tetrahymena* ribozyme. *Biochemistry* **1993**, *32*, 5291−5300.
(52) Uchida, T.; He, Q.; Ralston, C. Y.; Brenowitz, M.; Chance, M. R. Linkage of monovalent and divalent ion binding in the folding of the P4−P6 domain of the *Tetrahymena* ribozyme. *Biochemistry* **2002**, *41*, 5799−5806.
(53) Rohs, R.; Etchebest, C.; Lavery, R. Unraveling proteins: A molecular mechanics study. *Biophys. J.* **1999**, *76*, 2760−2768.
(54) Misra, V. K.; Draper, D. E. The linkage between magnesium binding and RNA folding. *J. Mol. Biol.* **2002**, *317*, 507−521.
(55) Grilley, D.; Soto, A. M.; Draper, D. E. Mg^{2+} RNA interaction free energies and their relationship to the folding of RNA tertiary structures. *Proc. Natl. Acad. Sci. U. S. A.* **2006**, *103*, 14003−14008.
(56) Romer, R.; Hach, R. tRNA conformation and magnesium binding. A study of a yeast phenylalanine-specific tRNA by a fluorescent indicator and differential melting curves. *Eur. J. Biochem.* **1975**, *55*, 271−284.